QUANTIFYING MORPHOLOGICAL CHARACTERISTICS OF ARCTIC AND SUB-ARCTIC MEANDERING RIVERS USING REMOTE SENSING

A Thesis

by

YAIR ISMAEL TORRES

Submitted to the Graduate and Professional School of
Texas A&M University
in partial fulfillment of the requirements for the degree of

MASTER OF SCIENCE

Chair of Committee,	Inci Guneralp
Committee Members,	Anthony Filippi
	Huilin Gao
Head of Department,	David Cairns

May 2022

Major Subject: Geography

ABSTRACT

A fundamental understanding of how river morphology interacts with permafrost is needed to understand the role of Arctic rivers as indicators and drivers of landscape change and their linkages to pan-Arctic feedback systems. Given the ecological role of rivers, projected changes in surface air temperatures, permafrost degradation, and hydrologic regimes, an investigation into the fundamental geomorphic dynamics of Arctic rivers and how those dynamics might be affected in the future is needed. For these reasons, the purpose of this study is to investigate the morphological characteristics of Arctic and sub-Arctic meandering river bends using remote sensing technology to determine whether the observed patterns have any relation to the areal extent of permafrost. A morphometric analysis using the bend and chord length, sinuosity, absolute average curvature, and asymmetry index of approximately 600 Arctic and sub-Arctic river bends indicates that bends from the continuous permafrost zones, discontinuous permafrost zones, and high-latitude non-permafrost regions are morphometrically different from one another at a half-meander bend scale. Results show that bends from the continuous permafrost zone, when compared to other bends from Arctic or sub-Arctic rivers, are statistically more likely to be 1) smaller in size (via chord and bend length), 2) have a lower chance of being upstream skewed (via asymmetry index) and 3) on average have sharper bends and sharp transition zones between bends (via absolute average curvature). However, the combination of the half-meander bend morphometrics when transformed via PCA, are alone not enough to delineate between river bends of different permafrost zones. This analysis reveals the unique morphometric signature of Arctic river bends and moves us closer towards understanding the control of permafrost on rivers.

ACKNOWLEDGEMENTS

I would like to thank my committee chair, Dr. Guneralp, and my committee members, Dr. Filippi, Dr. Gao, for their advisership and support throughout the course of this research. Thanks also go to my friends and colleagues in the Fluvial Landscapes and Dynamics Research Group for their assistance with the theory behind and the development of this research.

CONTRIBUTORS AND FUNDING SOURCES

Contributors

This research was supervised by a thesis committee consisting of Dr. Guneralp and Dr. Filippi of the Department of Geography and Dr. Gao of the Department of Civil and Environmental Engineering.

The python scripts utilized in this research were developed and provided by Billy Hales of the Fluvial Landscapes and Dynamics Research Group at Texas A&M University.

All other work was completed by the student, Yair Torres, independently.

Funding Sources

Graduate study was supported in part by a fellowship from Texas A&M University from the Graduate and Professional School and by funding from the Department of Geography for graduate assistant work.

TABLE OF CONTENTS

CHAPTER Page

LIST OF FIGURES

Page

LIST OF TABLES

Page

CHAPTER I

INTRODUCTION

Meandering rivers are intimately connected to their floodplains. Through their migration across landscapes, they play a large role in sediment transport (Zinger, Rhoads, and Best 2011), shaping the architecture of their floodplains (Lauer and Parker 2008a), and dictating floodplain connectivity (Castillo et al. 2020). Because of their unique relationships with floodplains, meandering river channels can act as indicators of widespread geomorphic and ecosystem changes. Furthermore, as ecological corridors between land and ocean, rivers are uniquely sensitive to the many interrelated consequences of climate change (Nijssen et al. 2001). Their sensitivity is particularly evident in systems undergoing rapid alteration, such as the Arctic, where warming is occuring at a rate of more than double the global average (Ballinger et al. 2020) and continuing the trend of Arctic amplification (Serreze and Barry 2011). With this increased warming, there have been concurrent declines in snow cover (Mudryk et al. 2017), increases in permafrost temperatures (Biskaborn et al. 2019), shifts in vegetation (Epstein, Myers-Smith, and Walker 2013; Bjorkman et al. 2020; Rew et al. 2020), and an intensification of the freshwater cycle (Rawlins et al. 2010). Models predict that the current extent of near-surface permafrost will be reduced by 2.1 million kilometers^2 or 10 million kilometers^2, under Representative Concentration Pathways (RCP) 2.6 and RCP 8.5, respectively (Arzhanov, Eliseev, and Mokhov 2013). RCP scenarios are different greenhouse gas concentration and climate policy scenarios defined by the Intergovernmental Panel on Climate Change (IPCC), where RCP 2.6 is the most stringent mitigation scenario and RCP 8.5 the least (IPCC 2013). Such degradation of permafrost poses risks to existing Arctic infrastructures (Hjort et al. 2018)

and the global economy, with pulses of methane released by thawing permafrost modelled to have an estimated global cost in the trillions of dollars for mitigation and adaptation measures (Whiteman, Hope, and Wadhams 2013). These high-impact changes, among others, will fundamentally alter the role of Arctic rivers as drivers and indicators of landscape change, and how Arctic rivers are viewed within the context of pan-Arctic feedback systems.

Increased efforts have been made to study the role of Arctic rivers as indicators of landscape change, with a primary focus on their hydrology. This is partially driven by the fact that despite the Arctic Ocean only accounting for approximately 1% of the global ocean volume, it receives about 10% of global river discharge (Dai and Trenberth 2002). Studies have documented increases in discharge (Peterson et al. 2002; J. W. McClelland et al. 2004; James W. McClelland et al. 2006; Holmes et al. 2018; Holmes et al. 2021) and changes in river biogeochemistry due to permafrost thaw (Frey and McClelland 2009; Wild et al. 2019). Peterson et al. (2002) found that the discharge from the six largest rivers in Eurasia to the Arctic Ocean increased by 7% from 1936 to 1999 and was positively correlated with mean surface air temperatures. This trend has continued into the 21st century with the combined discharge in 2020 of the 8 largest Arctic rivers being ~12% greater than the average discharge of these rivers for the reference period of 1981 to 2010 (Holmes et al. 2021).

Alternatively, Zheng et al. (2019) highlights the influence of rivers as drivers of change by modeling the impact of river inundation and discharge on permafrost degradation. Their results indicate that increased river discharge can impact the thermal state of subsurface permafrost and as a result deepen the topmost layer of permafrost that thaws seasonally. In terms of riverine and terrestrial freshwater systems, one of the largest impacts of permafrost thaw and degradation will be the transition from a surface-dominated system to a ground-water dominated

system (Frey and McClelland 2009). This in turn will likely have consequences on hydraulic connectivity, river discharge, and river migration and evolution, and further increase the role of rivers as drivers of change in a positive feedback loop. Despite the growing knowledge of changes occuring in Arctic river systems and to their surrounding landscapes, relatively little is known about the geomorphology and dynamics of Arctic rivers (Lininger and Wohl 2019) and the role of permafrost characteristics on the form and shape that rivers take. This is in part due to the belief that high-latitude rivers are structurally more stable and resistant to change than their lower-latitude counterparts because of the presence of permafrost (Scott 1978). It is likely that this perception will change with the increased thawing and degradation of permafrost, the collapse and slumping of river bends, and potentially the increased lateral migration of rivers.

Past studies examining the morphologies of river channels have often used morphometrics to help inform the theories regarding the dynamics of rivers (Leopold and Wolman 1960; Schumm 1967; Leeder 1973; Howard and Hemberger 1991; Stølum 1998; Ielpi et al. 2017; Finotello et al. 2020; Frasson et al. 2019). Morphometrics are defined here as metrics that measure some aspect of the morphology of a river. Critically, Howard and Hemberger (1991) provides a blueprint for the utilization of morphometrics to quantify the morphological similarities and differences between groups of rivers. For example, Finotello et al. (2020) conducted a similar multivariate analysis using morphometrics to highlight the differences in the morphologies of tidal and fluvial rivers. However, to my knowledge these methods have not been extensively used to investigate Arctic river dynamics across permafrost zones. The studies referenced dominantly focus on mid-to-low latitude regions or do not account for the potential influence of permafrost on the morphology of rivers. Collectively, this has resulted in a critical

gap in the knowledge and theory behind Arctic and sub-Arctic river morphodynamics and how these dynamics relate to their surrounding environment.

A fundamental understanding of how river morphology interacts with permafrost is needed to understand the role of Arctic rivers as indicators and drivers of landscape change and their linkages to pan-Arctic feedback systems. Given the ecological role of rivers, projected changes in surface air temperatures (Overland et al. 2019), permafrost degradation (Arzhanov, Eliseev, and Mokhov 2013), hydrologic regimes (Haine et al. 2015; Lique et al. 2016), and precipitation patterns (X. Zhang et al. 2013; Bintanja and Andry 2017), now is the time to investigate the fundamental geomorphic dynamics of Arctic rivers and how those dynamics might be affected in the future. For these reasons, the purpose of this study is to investigate the morphological characteristics of Arctic and sub-Arctic meandering river bends using remote sensing technology to determine whether the observed patterns have any relation to the areal extent of permafrost. I hypothesize that river bends in regions with a higher areal extent of permafrost have different morphological characteristics than those found in regions with less extent, or no permafrost at all. To test this, the study's two objectives are. 1) delineate river centerlines using Geographic Information Systems (GIS) and remote sensing, and using these centerlines, 2) quantify the morphological characteristics of half-meander river bends through a set of morphometrics. Successfully completing this analysis would reveal the unique morphometric signature of Arctic river bends and move us towards developing a deeper understanding of the control of permafrost on these signatures. Furthermore, filling this knowledge gap will result in an improved ability to contextualize riverine responses to current and future Arctic changes.

CHAPTER II

LITERATURE REVIEW

Arctic Environment & Permafrost Mapping

The Arctic and sub-Arctic are the northernmost regions of the Earth. They do not have exact geographic extents but are often defined using various regional characteristics such as precipitation, temperature, or vegetation. As such, exact extents can vary according to the field of study and cryosphere component covered (Love 1970). A conventional approach is to define the Arctic as the region north of the Arctic Circle (~66°5”), however definitions for sub-Arctic vary more widely. In this study, the areal extent of permafrost takes priority over specific Arctic or sub-Arctic definitions. Thus, I loosely define the Arctic as the region north of the Arctic Circle (~66°5”), and sub-Arctic as the region extending south from the Arctic Circle towards 50° N. It is important to note, however, that studies cited in this work each have their own definitions of the Arctic and sub-Arctic regions corresponding with their field of study.

The Arctic and sub-Arctic have Köppen-Geiger climates of polar and cold (Beck et al. 2018), respectively. Surface air temperatures can vary greatly across regions and seasons, but generally January is the coldest month and July is the warmest (Rigor, Colony, and Martin 2000). Furthermore, the Arctic is characterized as a treeless region dominated by shrubs, graminoids, and wetlands (Raynolds et al. 2019), whereas the sub-Arctic is composed of mostly boreal forest. In total, the Arctic and sub-Arctic regions extend to cover parts of the U.S, Canada, Russia, Greenland, Iceland, and northern Europe.

Arctic and sub-Arctic regions are undergoing rapid physical changes driven by climate change. A significant indicator of this is the continued warming of the Arctic, where warming is

occuring at a rate of more than double the global average (Ballinger et al. 2020) and continuing the trend of Arctic amplification (Serreze and Barry 2011). Arctic amplification is the theory that changes in global temperatures occur more extremely at high latitudes. Due to both positive and negative feedbacks between surface air temperature and other environmental variables, there are many observable changes to the biophysical state of the Arctic. One of the most visible examples of change is the decline of sea ice thickness (Kwok and Rothrock 2009) and cover (Cavalieri and Parkinson 2012; Stroeve et al. 2012) in the Arctic Ocean. Alternatively, with increased warming there has been vegetation greening trends across the pan-Arctic (Bhatt et al. 2010; Jenkins et al. 2020) and an extension of the growing season both from an earlier start date and a later end date (Zeng, Jia, and Epstein 2011; Jenkins et al. 2020). There are also indicators that the Arctic hydrological cycle has intensified (Rawlins et al. 2010) and will continue to intensity across the 21st-century (Kattsov et al. 2007; Lique et al. 2016) with localized warming being the primary driver of increased precipitation (Bintanja and Selten 2014; Bintanja 2018). Changes to the Arctic's freshwater system will have effects on and feedbacks to the ocean, atmosphere, ecosystems, and natural resources (Prowse et al. 2015). Collectively, changes in sea ice, air temperatures, and precipitation indicate that a 'new Arctic' is on the horizon (Landrum and Holland 2020).

One of the defining characteristics of the Arctic is the presence of permafrost. Permafrost is sub-surface material that remains at or below freezing temperature for two or more consecutive years (Harris et al. 1988). Permafrost is estimated to underlie ~24% of the exposed land area in the Northern Hemisphere (T. Zhang et al. 1999), and stores large amounts of carbon (Hugelius et al. 2014). The practice of mapping permafrost, regardless of spatial scale, is heavily limited by direct field data on the existence of permafrost and is therefore often supplemented

with climatic and environmental data to interpolate and extrapolate permafrost characteristics (J.A. Heginbottom 2002). There are various attributes of permafrost that can be mapped, including: continuity, thickness, temperature, ice-content, and its' geophysical, thermal, and engineering properties (J.A. Heginbottom 2002). It is most commonly characterized by its areal extent, or in other words the percent of ground that is underlain by permafrost. The widely accepted categories (zones) are continuous (90-100%), discontinuous (50-90%), sporadic (10-50%), and isolated (0-10%) (Brown et al. 2002). Depending on the methodology used to map or model permafrost, the areal extent zones can vary between permafrost map products.

Arguably the most widely used permafrost map is the Circum-Arctic map of permafrost and ground-ice conditions 1:10,000,000 (Brown et al. 1997). It was derived using existing physiographic or landscape maps across Russia, Alaska, and Canada, and depicts the extent of permafrost by percent area (areal extent) across the Northern Hemisphere and down to ~20° N latitude (J. Heginbottom et al. 1993). The map was a significant achievement, in that it was the first time that permafrost had been mapped for the entire circum-Arctic region using a common legend (J. Heginbottom et al. 1993). In 2002, a digital version of the map was generated in (Brown et al. 2002), allowing for its use and visualization in Geographic Information Systems (GIS). The map was gridded at 12.5-kilometer, 25 kilometer, and 0.5-degree resolution.

Given its ties with climatic feedback systems, the extent and change in extent of permafrost has been a key point of interest in the Arctic. Since the publication of Brown et al. (1997), studies have mapped the extent of permafrost across various spatiotemporal scales using a wide variety of methodologies and have often used Brown et al. (1997) as a reference point for their outputs. Obu et al. (2019) for example modeled and mapped the extent of permafrost in the northern Hemisphere based on a temperature at the top of permafrost (TTOP) based scheme.

This involved using land surface temperature, precipitation, tundra wetness, and landcover to model and calculate mean annual ground temperatures and the probability of permafrost. The result was the first high-resolution (1 kilometer^2) permafrost temperature and zonation map at a circum-Arctic scale that was based primarily on a remotely sensed dataset (Obu et al. 2019). Based on permafrost probabilities, the permafrost region extent is estimated at 20.8 x 10^6 kilometers^2, or 21.8% of the exposed land area. As of this analysis, the Obu et al. (2019) map is likely the most significant permafrost mapping product since the Brown et al. (1997) map.

Arctic River Changes and Environmental Controls

As previously mentioned, there have been observable increases in the discharge of Arctic rivers (Peterson et al. 2002; J. W. McClelland et al. 2004; James W. McClelland et al. 2006; Holmes et al. 2018; Holmes et al. 2021). The combined discharge of the 8 largest Arctic rivers was ~12% higher in 2020, than the average discharge of these rivers for the reference period of 1981 to 2010 (Holmes et al. 2021). In addition to increases in Arctic river discharge, observational and modeling studies indicate increases in river water temperatures (Liu et al. 2005; Park et al. 2020). This is particularly important given that river water temperature variability has been linked to surface air temperatures (Kaushal et al. 2010; van Vliet et al. 2011), and there is evidence that riverine heat fluxes are contributing to the downstream decline of Arctic Ocean sea ice (Dean et al. 1994; Whitefield et al. 2015; Park et al. 2020). For example, Park et al. (2020) found that river heat was responsible for 10% of the reduction in Arctic sea ice from 1980 to 2015. As such, it is likely that increasing surface air temperatures will in part drive an increase in riverine heat fluxes that ultimately impact the downstream ocean-sea ice-atmosphere heat budget (Park et al. 2020).

Increasing river discharge and water temperatures are also likely to have an impact on the formation and break up of river ice. A large portion of the Northern Hemisphere is affected by river ice (Bennett and Prowse 2010; Brooks, Prowse, and O'Connell 2013; Yang, Pavelsky, and Allen 2020), and although the duration of river ice varies regionally, the resultant breakup of river ice has vast ecological and hydrological impacts (Prowse 1994; Alfredsen 2017; Thellman et al. 2021). During the break-up of river ice, ice jams can form and lead to vast flooding. The combination of river ice break-up, ice-jam floods, and the resultant fluvial thermal erosion of banks (François Costard et al. 2014), indicate that river ice processes are a significant factor in the morphology and evolution of Arctic and sub-Arctic rivers.

This was previously noted by Heather, James, and Lee (2005) and more recently argued by James P. McNamara (2012). Based on the principles of hydraulic geometry and effective flow, James P. McNamara (2012) contends that river ice processes, similar to riparian vegetation processes, must affect major geomorphological measures and the equilibrium form of rivers. This contributes to the general hypothesis that Arctic environments and their processes have a control on the morphology of rivers. An example of a potential form of environmental control on the morphology of Arctic rivers, is the presence of permafrost. There is a general belief that the net effect of permafrost environments is to promote channel stability (Scott 1978). That being said permafrost region rivers have been described as having diverse fluvial processes and forms (Vandenberghe and Woo 2002). Furthermore, studies on permafrost region rivers have noted unique anomalies in their hydraulic geometries (J. P. McNamara and Kane 2009), and the influence of permafrost on the hydrological response of drainage basins (James P. McNamara, Kane, and Hinzman 1998, 1997) and the spatial organization of their channel networks (James P. McNamara, Kane, and Hinzman 1999). Although permafrost is very likely an environmental

control on the morphological expression of rivers, it is not well known as to how this control is expressed in the shape and form of river bends and across which permafrost zones it is expressed. This knowledge gap is further complicated by biophysical changes in the Arctic that will further alter the role of rivers as drivers and indicators of change, and ultimately their existing form. As an example, studies are increasingly documenting bank erosion along permafrost region rivers (F. Costard et al. 2003; Kanevskiy et al. 2016; Payne, Panda, and Prakash 2018; Fuchs et al. 2020).

River Bend Classification and Analysis

Meandering rivers can be subdivided into individual building blocks at various spatial scales (e.g., individual bend vs. river reach). Arguably the smallest geomorphic unit of a river is its' half-meander bends. Half-meander bends are defined as segments between two successive inflection points (i.e., points with zero curvature); where, two successive half-meanders constitute a full-meander. In this study, bend and half-meander are used interchangeably, and only refer to one individual bend, whereas full-meander refers to two consecutive bends.

Bends can take on various configurations and thus, there exist different classifications of meandering river bend types (Brice 1974; Frothingham and Rhoads 2003). Brice (1974) defined simple bends according to the relationship between the length and height of a bend, whereas Frothingham and Rhoads (2003) improves upon this definition by including criteria on the absolute angles of the channel path relative to the down valley direction. By doing so, Frothingham and Rhoads (2003) conforms bend type classifications to the dictionary definition of a loop. The terminology of bend types varies between classification types, however, the dominant characteristics described are the symmetry of bends and whether they are simple or complex (compound). A simple bend becomes compound if there is more than one dominant

curvature arc along its planform (Brice 1974). Visually this can be verified if there is more than one distinct lobe on a half-meander bend, or by qualitatively assessing how curvature changes along the path of a river bend. Where, simple bends will have one distinct curvature spike and a two-lobe compound bends will have two distinct curvature spikes. However, what qualifies as a distinct curvature arc/spike is somewhat subjective, therefore the visual distinction between simple and compound bends requires expert opinion.

According to Frothingham and Rhoads (2003) the four dominant bend types of meander rivers are: simple meander bends, elongate symmetrical meander loops, symmetrical compound meander loop, and asymmetrical compound meander loop. To simplify the classification of bends and to only focus on the half-meander bend scale, a revised bend classification scheme was utilized to classify half-meander bends using visual interpretation of bend planform and by qualitatively assessing each bend's curvature series. In this scheme all bend configurations were reduced to two bend types, simple bends or two-arc compound bends. Where simple bends are defined as only having one distinct curvature arc, and two-arc compound bends as having two distinct arcs. For further details regarding bend classification in this study see the Methods chapter.

Past studies examining the morphologies of river channels and their bends have often used morphometrics to help inform the theories regarding the dynamics of rivers (Leopold and Wolman 1960; Schumm 1967; Leeder 1973; Howard and Hemberger 1991; Stølum 1998; Ielpi et al. 2017; Finotello et al. 2020; Frasson et al. 2019). One of the early uses of morphometrics was to find the relationships between metrics across meandering river groups and to determine the general ranges of these values. For example, Leopold and Wolman (1960) analyzes the ratios between meander length and channel width and meander length and mean radius of curvature for

meander bends of flume rivers, meanders of Gulf Stream, and meanders on glacier ice. Schumm (1967) investigates the relationship between meander wavelength and discharge and sediment load, and finds that river wavelengths are dependent on both factors. Leeder (1973) uses empirical equations to relate bankfull width to bankfull depth. Studies like these helped form the foundational theory of bend morphology.

Although early studies using morphometrics found consistent and interesting relationships among the variables studied, studies like Howard and Hemberger (1991) called for the creation of more variables in order to relate the meandering patterns of rivers to controlling environmental patterns. As a result, Howard and Hemberger (1991) developed a suite of 40 morphometrics, joining existing morphometrics and newly created morphometrics, that could be measured from digitized river centerlines. The suite of morphometrics included measures of half-meanders statistics and ensemble averages for the entire channel. They applied these metrics to 57 sections of freely meandering channels and performed a factor analysis to determine how the channels related to one another. By doing so, Howard and Hemberger (1991) provides a blueprint for the utilization of morphometrics to quantify the morphological similarities and differences between groups of rivers.

More recently, studies such as Frascati and Lanzoni (2009) and Finotello et al. (2020) have used morphometrics and principal component analysis to compare different kinds of river types. Following after Howard and Hemberger (1991), Frascati and Lanzoni (2009) developed a suite of 12 morphometrics variables to compare natural rivers with mathematically modeled rivers. The suite of 12 morphometrics includes measures of half-meander and reach sinuosity, half-meander wavelength statistics (i.e., variance, skewness, kurtosis), distribution statistics of local curvature, and measures of asymmetry. Similarly, Finotello et al. (2020) developed a suite

of 20 morphometrics to highlight the differences in the morphologies of tidal and fluvial rivers world-wide. The suite consisted of sinuosity, intrinsic wavelength, curvature, and asymmetry, as well as their statistical moments (average, variance, standard deviation, skewness, and kurtosis).

Howard and Hemberger (1991), Frascati and Lanzoni (2009), and Finotello et al. (2020) show that the use of morphometrics, in the context of multivariate analyses, provide quantitative measurements of channel/bend shape and form and provide insights into the evolution and dynamics of river processes. These studies, along with those referenced earlier for their use of morphometrics to help inform the theories regarding the dynamics of rivers, dominantly focus on mid-to-low latitude regions or do not account for the potential influence of permafrost on the morphology of their river sites. Furthermore, to my knowledge morphometrics and multivariate analyses have not been extensively used to investigate Arctic river dynamics. Even global studies on the relationships between morphometrics such as Frasson et al. (2019), have failed to include high-latitude rivers in their analysis by only analyzing rivers between 60° N and 56° S. Collectively, this has resulted in a critical gap in the knowledge of Arctic and sub-Arctic river morphodynamics and how these dynamics relate to controlling environmental patterns (e.g., permafrost).

Remote Sensing of Channel Planforms

The use of remote sensing technology has been vital in studying fluvial environments (Marcus and Fonstad 2010). With the increased availability of medium to high resolution imagery, many studies have increasingly used imagery to quantify channel characteristics and dynamics (Güneralp, Filippi, and Hales 2014; Rowland et al. 2016; Schwenk et al. 2017; Finotello et al. 2020; Ielpi et al. 2017). The two primary methods of delineating channel planforms from imagery are through manual digitization in GIS or through some form of image

classification where the channel planform is extracted. Finotello et al. (2020) for example digitized 38 rivers and 58 tidal channels worldwide to morphometrically compare tidal and fluvial rivers. Alternatively, Allen and Pavelsky (2015) utilized a modified normalized difference water index formula and satellite imagery to create binary land-water masks and later extracted channel width data for all medium-to-large rivers in North America. Both methods provide unique qualities which make them favorable depending on the analysis. While image classification allows for the potential of automation, manual digitization arguably provides the highest level of user control in delineating channel planforms.

With the increased use of imagery for quantifying channel characteristics, there have been product developments that help automate the delineation of channel planforms and the measurements of channel characteristics. The National Center for Earth-Surface Dynamics (NCED) Channel Planform Statistics Toolbox developed by J. Wesley Lauer (and as used in Lauer and Parker (2008b)) is an ESRI ArcGIS 10.x add-in that can generate a centerline from two input digitized banklines. It does this by interpolating the center between the two banklines at points along the channel. The spacing of the points (nodes) along the channel is determined by a user specified distance. This results in river centerlines that are composed of equally spaced nodes.

RivWidth by Pavelsky and Smith (2008) is an IDL-based algorithm that generates river centerlines from raster-based classifications of channel area and orthogonal width transects at each centerline pixel. The tool was an improvement on manual measurements of channel widths from remotely sensed imagery and had comparable results to manual techniques (Pavelsky and Smith 2008). Fisher, Bookhagen, and Amos (2013) developed a methodology, ChanGeom, for extracting channel width and centerline datasets using high-resolution imagery of single-threaded

rivers from Google Earth and Bing Maps. The MATLAB-based ChanGeom acts as a counter-method to the IDL-based RivWidth algorithm presented in Pavelsky and Smith (2008), with a higher computational efficiency in measuring widths and centerlines for single-threaded channels (Fisher, Bookhagen, and Amos 2013). The method utilizes digitized or spectrally identified channel polygons to generate channel planform geometries. The high-resolution channel centerlines improved the quantification of channel sinuosity, an important metric for understanding channel meandering.

Another MATLAB-based product, RivMAP (Schwenk et al. 2017), uses Landsat 5 and Landsat 7 30-meter imagery to quantify migration modes and rates, erosion and accretion areas, and change in channel widths using support vector machine classification models. Like previous methods referenced, it utilizes image classified channel masks to delineate channel planform. The RivMAP tool uses a centerline approach and not a bankline approach to make its calculations, therefore it is best suited for single-threaded river systems and not multi-threaded systems (Schwenk et al. 2017). In other words, the method calculates meander migration from a river centerline evolution perspective, and not based on riverbank evolution and dynamics. In contrast to Schwenk et al. (2017), Rowland et al. (2016) developed the Spatially Continuous Riverbank Erosion and Accretion Measurements (SCREAM) algorithms, a set of algorithms that calculate the changes in channel characteristics independent of the channel morphology from channel planform masks. This allows SCREAM to quantify planview river change of both single and multi-threaded river systems. The algorithms quantify erosion and accretion rates, area of change, area of island change, and channel width and bank curvature at bank pixels. Furthermore, SCREAM addresses the lack of methods able to quantify channel migration and erosion and accretion dynamics, from a bank-based reference frame and not a channel centerline

reference frame. This allows for an increased spatiotemporal investigation of channel dynamics at varying scales. Using the methods outlined in Rowland et al. (2016), Rowland and Stauffer (2019) published a dataset containing detailed planform metrics for 14 reaches of 13 Arctic rivers. The dataset spans from the 1970s to 2016 and covers 5,500 kilometers of Arctic rivers. To the best of my knowledge, this is the only existing Arctic river morphology dataset of its kind.

Although each of the tools discussed here provide valuable measurements of channel planforms and dynamics, no existing tool can automate each of the morphometric calculations required for this study's analysis, nor can they do it at a river bend scale. As a result, the existing Channel Planform Statistics Toolbox in combination with algorithms generated in-house from the Fluvial Landscapes and Dynamics Research Group at Texas A&M University were used to generate river centerlines and calculate channel planform characteristics. The NCED Channel Planform Statistics Toolbox was selected as the centerline generation method due to its easy use with manually digitized banklines and the ability to generate centerlines with equally spaced nodes based on a user-specified distance and not based on image pixels. This feature allows for the highest level of centerline customization, and later, the generation of width transects at each centerline node. Although this method relies on manual digitization and does not use image classification, the low number of study sites in this analysis and the ability to control the delineation of river margins made it the most feasible method. Detailed specifics on channel planform delineation from satellite imagery, centerline generation, and morphometric calculations can be found in the Methods chapter below.

CHAPTER III

STUDY SITES

To determine study sites for this research, I used the Allen and Pavelsky (2018) river centerline dataset and two permafrost maps of the Arctic. As mentioned previously, the areal extent of permafrost can vary between permafrost map products. To mitigate these differences, I overlaid the Circum-Arctic Map of Permafrost and Ground-Ice Conditions v2 (Brown et al. 2002) and the Obu et al. (2019) permafrost map on each other to identify locations where both maps agreed on the areal extent of permafrost (Figure 1).

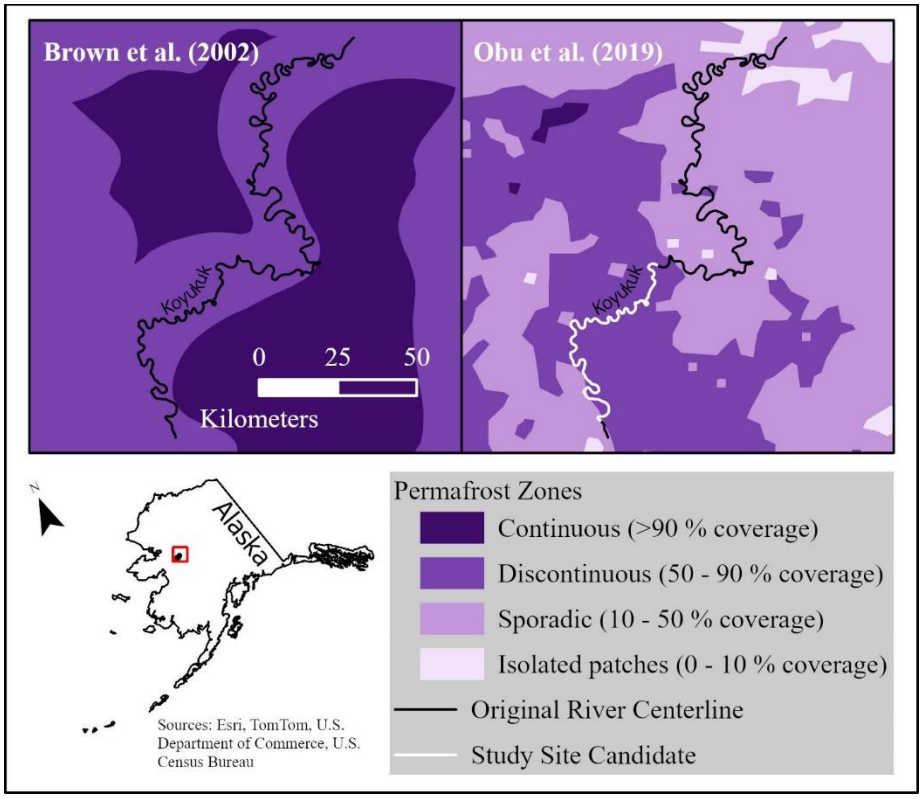

Figure 1: Two permafrost maps were used to identify river reaches in the same permafrost zones.

As can be seen in Figure 1, a reach of the Koyukuk River in Alaska, USA falls into two distinct permafrost zones, discontinuous and sporadic, depending on the permafrost map used. Only the portions of rivers that fell into the same permafrost zone across both the Brown et al. (2002) and Obu et al. (2019) maps were considered as potential study site candidates. Using these resources, I selected study sites based on the following criteria: (i) an average channel width wide enough to be appropriately captured in Landsat satellite imagery, (ii) floodplain permafrost extent, (iii) meandering character of the river, and (iv) the presence of a minimum meander train length of 15 bends. Preliminary average channel widths were estimated by measuring the channel width using GIS at random intervals across the reach of interest. I strictly focused on channels within the continuous and discontinuous permafrost zones, as well as reaches near but outside of isolated patches of permafrost. Furthermore, I did not consider river channels below the 50°N latitude as I deemed them outside of the generally accepted Arctic or sub-Arctic zones. The river and permafrost datasets were visualized in a Geographic Information System (GIS), ArcPro, and a total of nine reaches across Alaska and Russia were identified (Table 1, Figure 1). While the list of selected rivers is not exhaustive, the nine river reaches meet the criteria detailed above.

Alaskan Rivers

Four out of the nine river reaches are located across Alaska, USA, and have a combined length of approximately 440 kilometers (Table 1). All four reaches can be viewed in Figure 2 on page 30. The Itkillik River reach is located in the Beaufort Coastal Plains ecoregion of the Alaskan Tundra (Nowacki et al. 2003), just north of the Brooks Range, and drains into the Beaufort Sea. The reach is located within the continuous permafrost zone according to Brown et

al. (2002) and Obu et al. (2019) and has a total length of approximately 121 kilometers. The vegetation community surrounding the reach is described as moist tundra dominated by non-tussock and tussock sedges, dwarf-shrub, and moss tundra (Raynolds et al. 2019). The immediately surrounding region primarily has Gleysol soils with a loam texture (FAO et al. 2012). An estimate of the area's short-term (2017-2021) average surface air temperature is approximately -9 C°, and for winter (DJF) and summer (JJA), it's -23 C° and 7 C°, respectively (Station Deadhorse Ap, ID: USW00027406). Surface air temperature estimates for this area and for each of the following river areas were sourced from https://data.giss.nasa.gov/gistemp/station_data_v4_globe/, a dataset of NOAA GHCN v4 adjusted and homogenized meteorological stations used in GISS Surface Temperature Analysis v4 (GISTEMP-Team 2022; Lenssen et al. 2019). The closest NOAA GHCN v4 meteorological station with the most complete and recent data was used; however, it should be noted that on a station-by-station basis estimates are made from datasets with missing monthly data.

Table 1: List of the four Alaskan river reaches investigated in this study.

River	Permafrost Zone	Start (lon.,lat.)	End (lon.,lat.)	Total Length (kilometers)
Itkillik	Continuous	-151.087, 69.660	-150.926, 70.150	120.6
East Fork Chandalar	Continuous	-145.107, 68.445	-145.761, 68.051	109.6
Draanjik	Discontinuous	-144.051, 66.686	-144.73, 66.664	82.0
Koyukuk	Discontinuous	-156.828, 65.544	-157.66, 65.143	127.4

Moving southward and past the Brooks Range is the East Fork Chandalar (EFC) River reach. The EFC River reach is located in the Yukon River Lowlands ecoregion within the intermontane boreal region of Alaska (Nowacki et al. 2003). The reach is located within the

continuous permafrost zone according to Brown et al. (2002) and Obu et al. (2019) and has a total length of approximately 110 kilometers. The vegetation community ranges from sedges, shrubs, and moss/herb tundra (Raynolds et al. 2019) to sparse boreal forest (Nowacki et al. 2003). The immediately surrounding region primarily has Gleysol soils with a loam texture (FAO et al. 2012). An estimate of the area's short-term (2015-2017) average surface air temperature is approximately -4 C°, and for winter (DJF) and summer (JJA), it's -16 C° and 11 C°, respectively (Station Helmut Mountain, ID: USR0000AHEL).

Even further south is the Draanjik (Black) River reach site located primarily between Fort Yukon, Alaska and Chalkyitsik, Alaska. The river reach falls in the Alaskan intermontane boreal ecoregion of Yukon-Old Crow Basin (Nowacki et al. 2003). The reach is located within the discontinuous permafrost zone according to Brown et al. (2002) and Obu et al. (2019) and has a total length of approximately 82 kilometers. The vegetation community ranges from wet grass and shrub marshes to aspen-birch-spruce forests (Nowacki et al. 2003). The area has Gleysol soils with the dominant soil texture being loam (FAO et al. 2012). The short-term (2017-2021) average surface air temperature is approximately -5 C°, and for winter (DJF) and summer (JJA), it's -26 C° and 14 C°, respectively (Station Chalkyitsik Alaska, ID: USR0000ACHL).

The Koyukuk River reach is in west-central Alaska, south of the city of Huslia and east of the Nulato Hills. The reach is within the Alaskan intermontane boreal ecoregion of Yukon River Lowlands, an expansive wetland system (Nowacki et al. 2003). The reach is located within the discontinuous permafrost zone according to Brown et al. (2002) and Obu et al. (2019) and has a total length of approximately 127 kilometers. The surrounding vegetation community is largely composed of lowland boreal forests, shrubs, and sedges, (Nowacki et al. 2003). Similar to the other river reaches, the area primarily has Gleysol soil with a loam soil texture (FAO et al.

2012). The short-term (2019-2021) average surface air temperature is approximately -2 C° and for winter (DJF) and summer (JJA), it's -16 C° and 14 C°, respectively (Station Cottonwood Alaska, ID: USR0000ACOT).

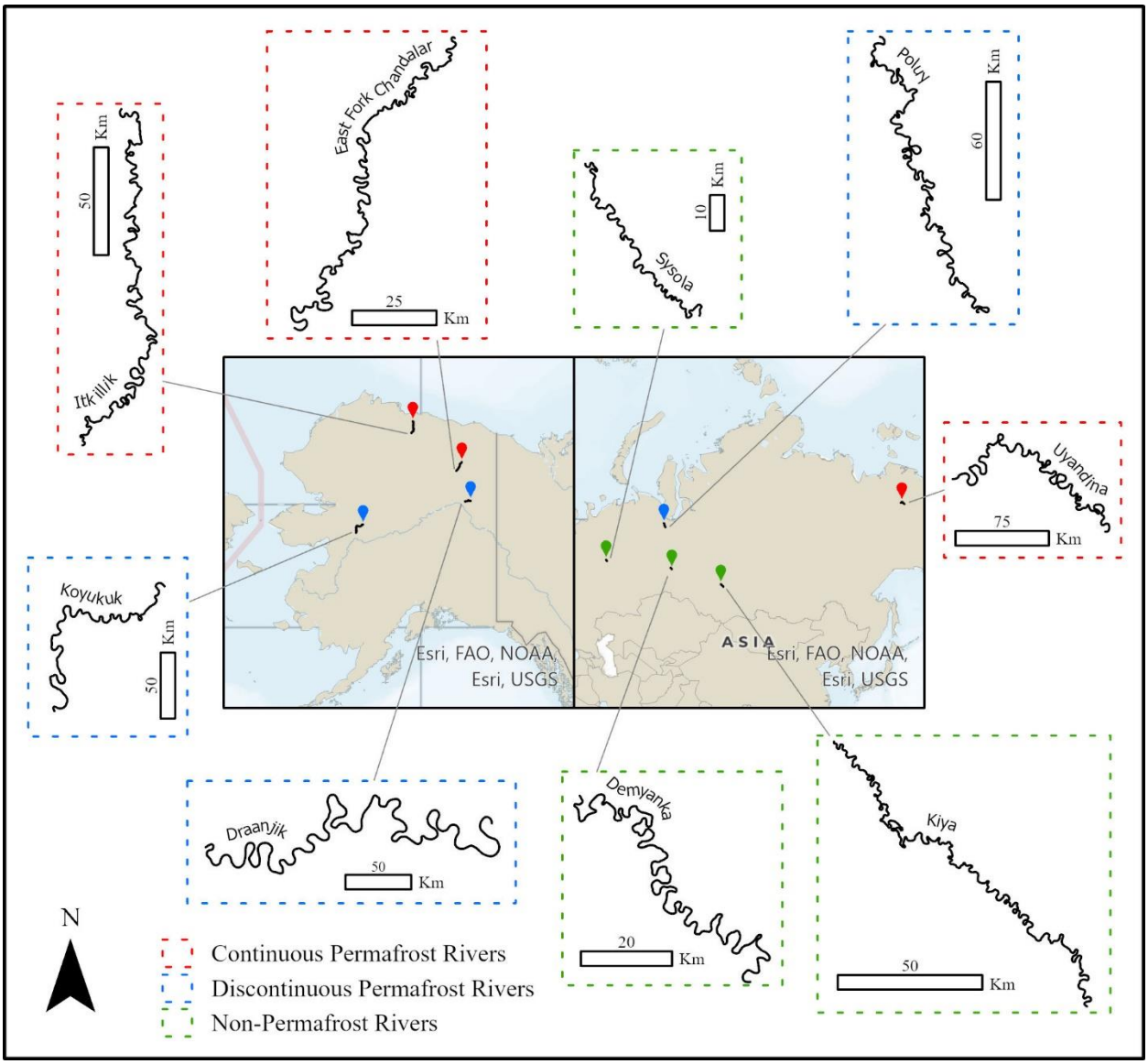

Figure 2: Location of river reaches investigated in this study. (Left) Four reaches are in Alaska, USA. (Right) Five reaches are in Russia.

Russian Rivers

Five out of the nine river reaches are located across Russia and have a combined length of approximately 613 kilometers (Table 2). All five reaches can be viewed in Figure 2 on page 30. The Uyandina River reach is in northeastern Russia in the northeastern part of the Sakha Republic and is east of the Chersky Mountain Range. The reach is located within the continuous permafrost zone according to Brown et al. (2002) and Obu et al. (2019) and has a total length of approximately 150 kilometers. The region is swampy and has often flooded vegetation with a mixture of needleleaf and evergreen forests (Sayre et al. 2014). The reach carves through Fluvisol soils that primarily have a sandy-loam texture, but is bordered by Gleysols and Histosols (FAO et al. 2012). The short-term (1986-1990) average surface air temperature is approximately -13 C° and for winter (DJF) and summer (JJA), it's -37 C° and 12 C°, respectively (Station Druzina, ID: RSM00024197).

Table 2: List of the four Russian river reaches investigated in this study.

River	Permafrost Zone	Start (lon.,lat.)	End (lon.,lat.)	Total Length (kilometers)
Uyandina	Continuous	144.637, 68.524	145.820, 68.403	150.3
Kiya	Non-Permafrost	87.806, 56.259	86.994, 56.742	159.0
Demyanka	Non-Permafrost	71.275, 59.264	70.907, 59.485	99.6
Poluy	Discontinuous	69.271, 65.474	68.771, 65.998	151.0
Sysola	Non-Permafrost	50.556, 60.571	50.246, 60.772	52.5

The Kiya River reach is in southern Russia and spans 159 kilometers across the northern portion of Kemerovo Oblast and southern portion of Tomsk Oblast. The reach is in the Western Siberian hemiboreal forests ecoregion, at the southernmost region of the Russian taiga (Olson et al. 2001), and outside any permafrost zone according to Brown et al. (2002) and Obu et al.

(2019). The vegetation community is primarily composed of mixed forests (Olson et al. 2001; Sayre et al. 2014). The area has Fluvisol soils that primarily have a sandy-loam texture, but is bordered by Greyzems and Podzol soils (FAO et al. 2012). The short-term (2017-2021) average surface air temperature is approximately 2 C° and for winter (DJF) and summer (JJA), it's -14 C° and 18 C°, respectively (Station Mariinsk, ID: RSM00029551).

The Demyanka River reach is in the southwestern portion of Russia in Tyumen Oblast and in the West Siberian taiga ecoregion (Olson et al. 2001). The reach is outside of any zone of permafrost according to Brown et al. (2002) and Obu et al. (2019) and spans approximately 100 kilometers. The vegetation community is primarily characterized by mixed forest and some grassland, scrub, and shrub landscapes (Olson et al. 2001). The reach meanders through Fluvisol soils that primarily have a sandy-loam texture (FAO et al. 2012). The short-term (2017-2021) average surface air temperature is approximately 1 C° and for winter (DJF) and summer (JJA), it's -17 C° and 17 C°, respectively (Station Demjanskoe, ID: RSM00028076).

The Poluy River reach is in northwestern Russia in Tyumen Oblast and east of the Ural Mountains. Similar to the Demyanka River reach, the Poluy River reach is outside of any permafrost zone according to Brown et al. (2002) and Obu et al. (2019), and is also in the West Siberian taiga ecoregion (Olson et al. 2001). The area has swampy often flooded vegetation and needleleaf/evergreen forests (Sayre et al. 2014), and Fluvisol soils with a dominant soil texture of sandy-loam, but is bordered by Gleysols and Histosols (FAO et al. 2012). The total length of the reach studied is 151 kilometers. The short-term (2017-2021) average surface air temperature is approximately -4 C° and for winter (DJF) and summer (JJA), it's -21 C° and 13 C°, respectively (Station Salekhard, ID: RSM00023330).

The Sysola River reach is in northwestern Russia in the Komi Republic, west of the Ural Mountains. It is within the Scandinavian and Russian taiga ecoregion, surrounded by hills (Olson et al. 2001), and spans 53 kilometers in length. The vegetation community is mostly needleleaf/evergreen forests and deciduous forests (Sayre et al. 2014), and the area has Fluvisol soils with a sandy-loam texture, but is surrounded by Podzol soils (FAO et al. 2012). The short-term (2014-2018) average surface air temperature is approximately 2 C° and for winter (DJF) and summer (JJA), it's -11 C° and 16 C°, respectively (Station Koigorodok, ID: RSM00023904).

CHAPTER IV

METHODS

The analyses of Arctic and sub-Arctic river half-meanders using morphometrics was conducted in four major steps:

1. Delineation of river area and generation of river centerlines from remotely sensed imagery.
2. Identification of individual half-meander bends using bend curvature data and expert opinion.
3. Application of a suite of morphometrics to identified half-meander bends.
4. A multivariate analysis of bend morphometric data.

Steps 1-3 are outlined below, and details of Step 4 can be found in the Results chapter.

River Centerline Generation

River planform data were extracted by digitizing channel banks from satellite imagery. Landsat 8 OLI – Collection 1 – Level 1 – Tier 1 imagery was acquired from the USGS Earth Resources Observation and Science Center Landsat archive. This imagery was used due to it being the highest quality available Landsat imagery at the time of data collection with a georegistration accuracy of less than or equal to a 12-meter radial root mean square error. Criteria for selecting imagery was based on lack of cloud cover (<10%), a terrain precision correction, nadir satellite positioning, and whether a given image was captured during the summer months (May – August) of 2018 and 2019. The summer period was selected to increase the significant/maximal vegetation cover available for river versus non-river delineation. One image was selected for each of the nine river reaches (Table 3).

Table 3: Landsat 8 OLI Imagery Used

River	Image ID
East Fork Chandalar	LC08_L1TP_070012_20190626_20190705_01_T1
Itkillik	LC08_L1TP_076011_20190807_20190820_01_T1
Uyandina	LC08_L1TP_115012_20190622_20190704_01_T1
Draanjik	LC08_L1TP_068013_20190831_20190916_01_T1
Koyukuk	LC08_L1TP_075014_20190613_20190619_01_T1
Poluy	LC08_L1TP_163014_20190724_20190801_01_T1
Demyanka	LC08_L1TP_158019_20190822_20190903_01_T1
Kiya	LC08_L1TP_146021_20190802_20190819_01_T1
Sysola	LC08_L1TP_172018_20180517_20180604_01_T1

The riverbanks for each reach were digitized as polylines in ArcPro 2.6.2. The river channel was defined as the area between vegetation lines on either bank, assuming that non-vegetated areas in-between vegetation lines are inundated for parts of the year. The spatial resolution/spacing of the points on the polylines was roughly equivalent to the mean channel width; although, the resolution was increased in areas of high curvature and/or high variability in channel width to capture the necessary morphological details. The mean channel width was estimated for each river by polygonising the river area from two river banklines and dividing the area by the average length of the two banklines. River centerlines were generated with the NCED Channel Planform Statistics Toolbox using the banklines of each of the nine rivers, such that the centerline spacing of any given river was equivalent to ½ mean channel width (Ex: Itkillik average channel width = 172 m, centerline spacing = 86 m). A spacing of ½ mean channel width was used to ensure that the morphologic complexity of each channel planform was captured in

the centerline, without distorting the resultant curvature signature. This was retroactively verified by testing different centerline spacings and quality checking curvature signatures.

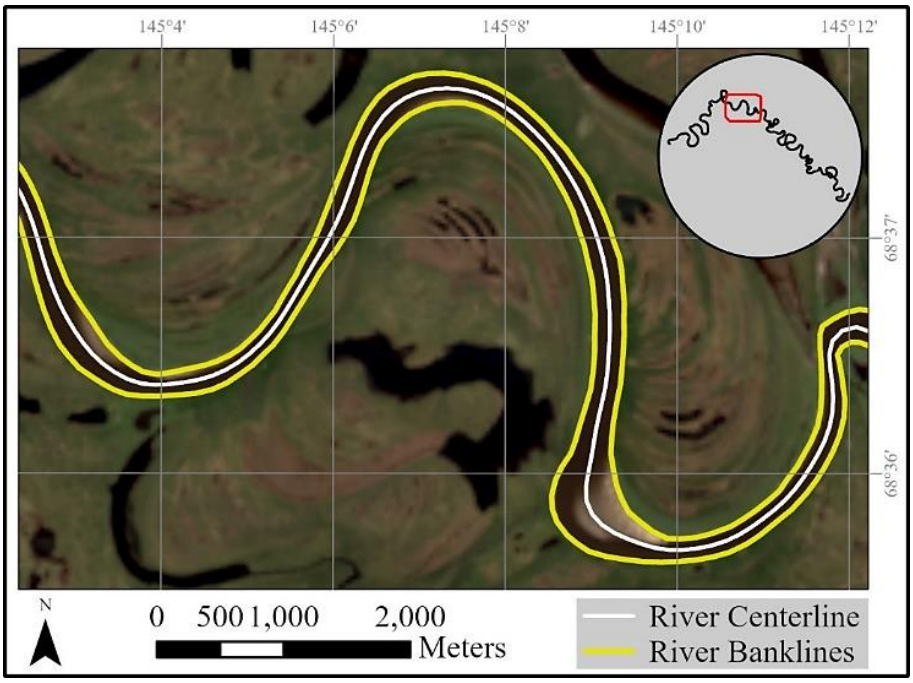

Figure 3: Banklines and centerline of the Uyandina river. Banklines were manually digitized in ArcPro and the centerline was generated using the Channel Planform Statistics tool (NCED). The centerline was smoothed and resampled at a ½ avg. channel width.

The centerline nodes were then smoothed with a Savitzky-Golay (S-G) filter with a kernel size of 7 nodes and a power of 5 three times (Hamming 1983; Fagherazzi, Gabet, and Furbish 2004) to reduce any digitizing noise or artifacts. The S-G filter replaces the location of each node with a smoothed representation of the neighboring nodes within the kernel; therefore, the new nodes on the resulting centerlines are no longer equally spaced. To address this issue, the python script *line_resample*, developed by the Fluvial Landscapes and Dynamics Research Group (FLUD) at Texas A&M University-Geography, was used to resample the smoothed

centerlines back to their original spacing of ½ mean channel width. The *line_resample* script, as well as the ones mentioned below, utilize the propy.bat ArcPro file to activate the ArcGIS Pro conda environment and run stand-alone scripts directly from a Microsoft Windows' Command Prompt. The resampling script creates a buffer around the first centerline node and creates a new node at the location of the buffer's intersection with the original centerline. The size of the buffer is user-specified (e.g., ½ mean channel width). The script repeats this process at each new node until a new centerline is generated (Figure 3).

Using the FLUD-developed python script *generate_curvature*, curvature was calculated at each smooth, equally-spaced, centerline node (Figure 4) to generate a curvature series for all nine river centerlines.

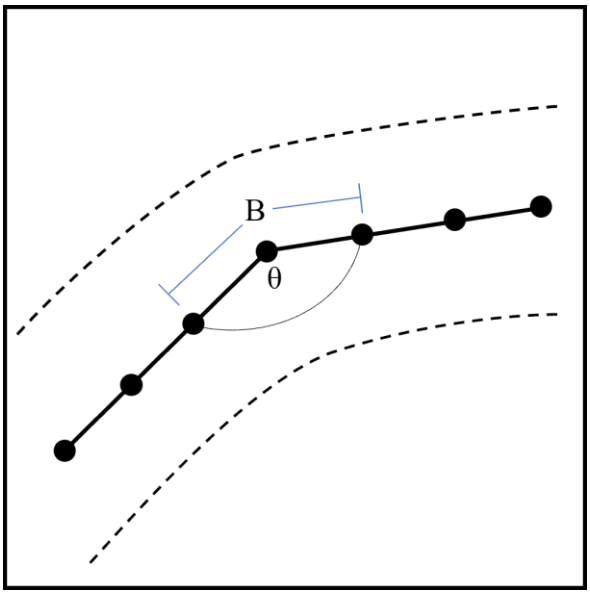

Figure 4: Curvature was calculated at each river centerline node (black circle) as the smaller of the angles created by adjacent centerline segments (black solid lines), θ, divided by the combined lengths of the two segments, B.

Curvature, *C*, is defined as:

$$C = \frac{\theta}{B} \qquad \textbf{Eq. 1}$$

where, θ is the smaller of the two angles created between two (three) consecutive centerline segments (nodes) and *B* is the combined length of the two segments. By default, curvature is not computed at the first and last centerline node, since a downstream and upstream centerline segment are required for the calculation.

River Bend Identification

The identification of individual river bends was based on inflection points, represented as changes in the curvature sign (+ or -) between groups of nodes, wherein, a change in curvature sign results in the beginning or end of a bend (Figure 5). This was done in three processing steps, 1) reclassifying the original curvature series to eliminate small spurious regions of curvature, 2) the generation of bends based on the reclassified curvature series, and 3) the expert assessment and manual reclassification of generated bends.

First, the FLUD-developed python script *spurious_bends* was used to reclassify the original node curvature where needed. Reclassification of node curvature is required mostly in portions of the river that are straight or in the regions of transition from one bend to another, where there is low variation in curvature around zero. The script reads the original node curvature, identifies regions of small curvature, and changes the curvature sign of these small regions to match the sign of its neighboring nodes; essentially, creating a centerline segment of continuous positive or negative curvature. Regions of small curvature are determined by the user-specified node window size. For example, if a node window size of 3 is set, all regions with only 3 nodes or less of a positive or negative curvature sign, are changed to match their

neighbor's curvature sign. Each centerline was modified using an arbitrary node window size between 3 and 5, helping further clean the curvature series of any digitizing artifacts or noise. This node window size range was determined after investigating each river centerline and assessing trends in the length of small regions of curvature.

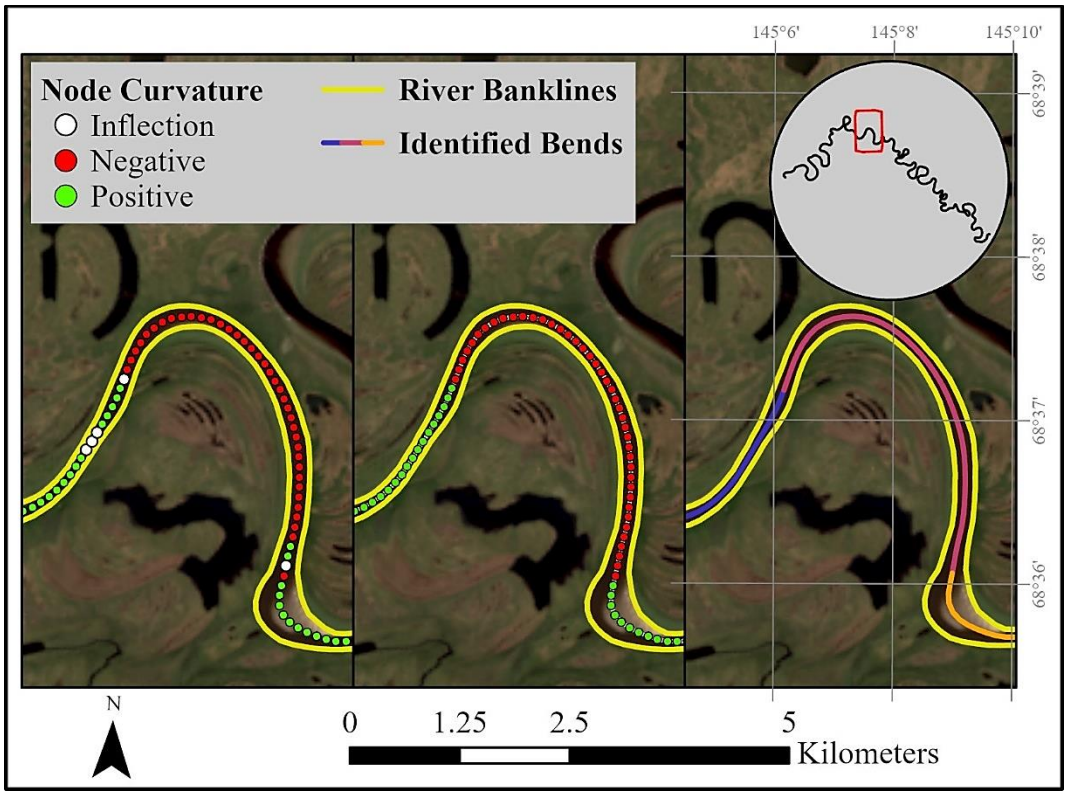

Figure 5: Bend identification based on node curvature. (Left) Raw node curvature with inflection points present. (Middle) Reclassified curvature series with small regions of curvature merged. (Right) Bend generation based on reclassified curvature.

Second, the FLUD-developed python script *generate_bends* was used to identify and generate individual river bends based on the reclassified centerline curvature series. The script evaluates the changes in the sign (+ or -) of the reclassified centerline curvature series, wherein, a change in curvature sign results in the beginning or end of a bend. This process results in a new

ArcGIS shapefile in the form of a bend-segmented polyline, where each segment represents a single bend.

Third, the script-identified bends were manually checked to ensure their agreement with expert opinion on what constitutes a bend and then classified by bend type. Manual inspection was conducted by visualizing the original unmodified curvature series, the reclassified curvature series, and the final bend-segmented centerlines in ArcPro. The definitions of river bends by Brice (1974) and Frothingham and Rhoads (2003) were referenced when identifying true bends. Although exact definitions of bend types differ between authors, a combination of their definitions along with expert opinion was used to filter centerline bends for two dominant bend types: simple and two-arc compound bends. Here, I loosely define simple bends as the simplest form of a bend, consisting of one clear curvature series arc. Two-arc compound bends are defined as two simple bends joined by a straight centerline segment no longer than ~6 centerline nodes (3 channel widths). Interestingly, expert opinion often identified a simple bend as a centerline segment with a length of at least five nodes (2.5 channel widths), with three consecutive centerline nodes above a mean channel-width normalized curvature value of |0.06|. Using these general guidelines and modified definitions of river bends, bends were manually identified for all nine river reaches.

Centerline bends were manually corrected for two primary geomorphic expressions: ‘straight’ river segments and multi-lobe (>2) compound bends. Because the curvature series is the product of manually digitized riverbanks, there is inherent noise in the series. As such, the script-identified bends often mis-identified bends in relatively straight reach segments where the curvature sign can change from node to node. In this study, relatively straight river segments were considered as one bend regardless of discrete curvature sign changes, unless if part of a

two-arc compound bend. Multi-lobe (>2) compound bends were filtered due to their incompatibility with asymmetry index calculations, a measure of bend skewness based on a single curvature maximum (i.e., upstream vs. downstream skewed). The asymmetry index equation is defined further below. Multi-lobe compound bends can have multiple curvature maxima and an asymmetry index calculation cannot accurately quantify overall bend skewness; thus, they were split into individual simple or two-arc compound bends according to sign changes in the curvature signature. Although two-arc compound bends can have two distinct curvature maximums, they are not filtered in this study because I argue that the dominant curvature maximum of such a bend is representative of overall bend skewness.

The final result of bend identification and classification was a polyline shapefile of each river centerline, segmented at each bend and classified into three categories, simple bends ('S'), two-arc compound ('C'), or discarded ('D'). The discarded bends ('D') are portions of the river that are straight or where the generation of width transects (explained further below) failed. The datasets were specifically designed this way to allow for filtering of bends based on classification (e.g., simple and two-arc compound bends only) in the statistical analyses done below.

Morphometric Variable Dataset

A set of morphometric variables commonly used in the literature was identified to objectively characterize river meander morphologies from half-meander bends. In addition to the previously calculated curvature series, these variables include measures of bend width, length, sinuosity, and asymmetry (Howard and Hemberger 1991; Finotello et al. 2020). Ensemble statistics were generated for the purposes of better understanding the characteristics of each river reach; however, the dominant focus of this study is at the half-meander bend-scale therefore only bend statistics are reported here and used in the statistical analyses.

At each centerline node, width transects were generated using the FLUD-developed script *generate_bends_widths*. The script takes a bend-segmented polyline shapefile and the bankline shapefiles and creates a bisecting line (i.e., width transect) for each node on each bend (Figure 6). The direction of each width transect is determined by measuring the smaller of the two angles created between adjacent centerline segments and dividing it in half. Then, 180° is added to that angle to cast a bisecting line in the opposite direction, completing the width transect for a node. To ensure that width transects intersect with the correct portion of the digitized banklines, a user-specified distance-buffer is used to limit the distance a transect can 'look' for a bankline intersection. By default, width transects are not computed at the first and last centerline node, since a downstream and upstream centerline segment are required for the calculation.

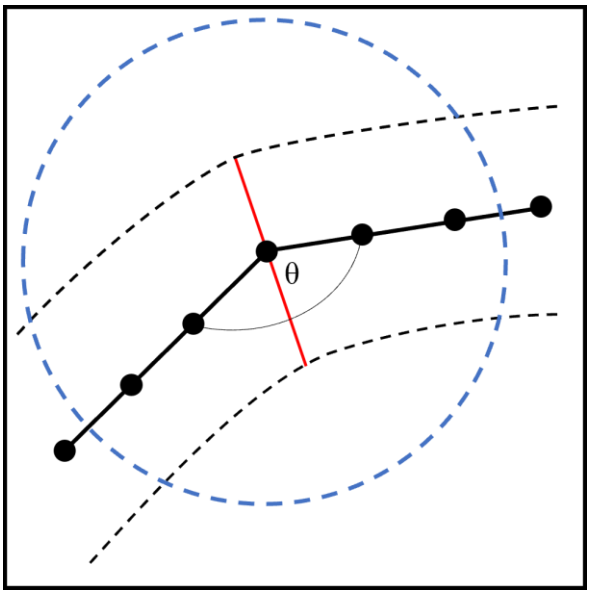

Figure 6: Width transects (red line) are cast out from each centerline node (black circles) in a direction equal to θ/2 (+180°) until it intersects with a digitized bankline (black dashed lines). A user-specified buffer (blue circle) limits the search window.

The *generate_bends_widths* script failed to successfully draw width transects at highly concave/convex bends, where the projection of transects bypassed neighboring banklines and connected to downstream or upstream banklines or failed to generate entirely (Figure 7). In relatively wide rivers with high curvature bends, the user-specified buffer must be large enough as to not limit the search window of the transects. As a result, a width transect has a large window to search for an intersection with a bankline, but no neighboring banklines to intersect with along its projected path. The bends where width transects failed to generate were classified as 'discarded' bends and were excluded from the statistical analyses below.

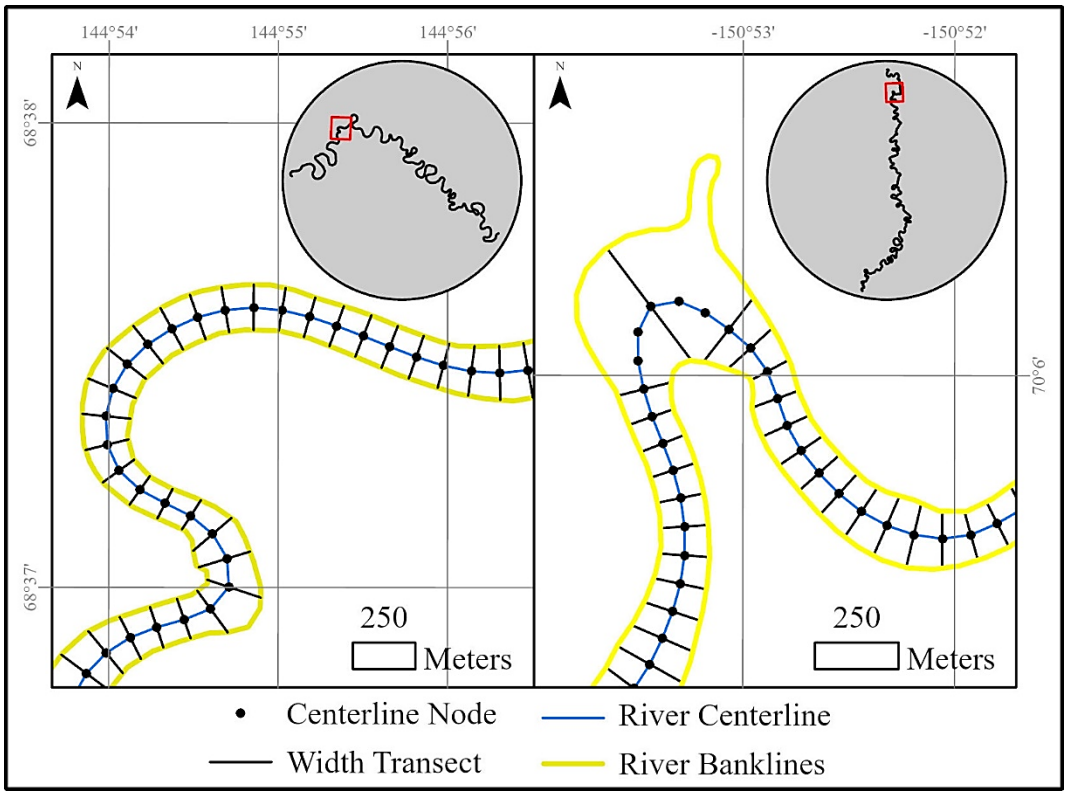

Figure 7: (Left) An example of width transects successfully generating on an Uyandina river bend. (Right) An example of width transects not generating correctly on a high-curvature bend of the Itkillik river.

In addition to generating width transects, the *generate_bends_widths* script also computes the minimum, average, maximum, and median width values for each bend and adds these data to the input bend-segmented centerline shapefile. To make the variables unitless and rivers of different sizes comparable, the average local bend width, W_{Av}, is used to normalize the bend statistics in the analyses done below.

Table 4: General morphometrics calculated by a FLUD-developed python script. Not included are the statistical moments calculated for curvature (average, variance, standard deviation, skewness, and kurtosis).

Morphometric		Defined As	Width Normalized Morphometric
Bend Length	*L*	Centerline (curvilinear) length of a bend	$L_* = L / W_{Av}$
Curvature	*C*	Inner angle between two tangents divided by summed length of tangents	$C_* = C * W_{Av}$
Sinuosity	*S*	Ratio between bend length and chord length	Unitless Not Normalized
Asymmetry Index	*A*	Measure of bend skewness based on location of bend curvature maximum	Unitless Not Normalized
Chord Length	*D*	Straight-line distance between start and end points of a bend	$D_* = D / W_{Av}$

The FLUD-developed script *bend_HH91_analysis* takes in a series of half-meander bends and generates statistics for each bend. These statistics consist of bend length, sinuosity, asymmetry index, chord length, and statistical moments of signed curvature and absolute curvature (average, variance, standard deviation, skewness, and kurtosis) (Table 4). Unlike the

other morphometrics, because curvature is calculated at every centerline node in each bend the statistical moments can be calculated for each bend.

Bend length, *L*, is defined as the centerline length of a river segment. An example of half-meander bend length can be seen in Figure 8.

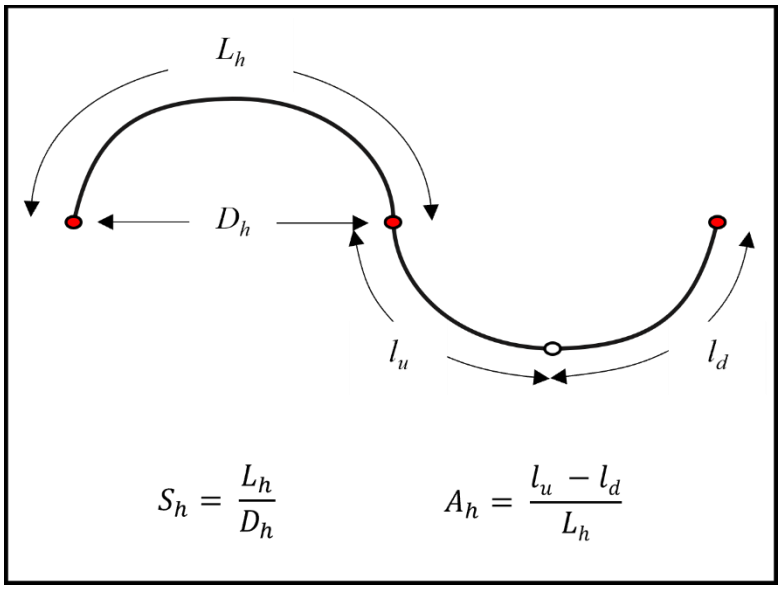

Figure 8: Diagram of the half-meander morphometrics generated (flow-direction right). In this example, the start and end (inflection) points of each half-meander bend are denoted by red dots and a theoretical curvature maximum by a white dot.

Bend length is normalized with the local average bend width W_{Av} (i.e., L / W_{Av}). Chord length, D_h, is defined as the straight-line distance between the start and end points of a half-meander bend, or in other words the distance between successive inflection points. Sinuosity is measured as the ratio between bend length and chord length. As such, half-meander sinuosity, S_h, is defined as:

$$S_h = \frac{L_h}{D_h} \qquad \textbf{Eq. 2}$$

Bend asymmetry, *A*, is a measure of bend skewness and is defined as:

$$A = \frac{l_u - l_d}{L} \quad \textbf{Eq. 3}$$

where, l_u and l_d are the distances from the curvature maximum to the upstream and downstream inflection points, respectively. As such, half-meander bend asymmetry, A_h, is defined as:

$$A_h = \frac{l_u - l_d}{L_h} \quad \textbf{Eq. 4}$$

As a result, upstream skewed bends have negative asymmetry values ($l_u < l_d$), and downstream skewed bends have positive values ($l_u > l_d$).

Once the bend morphometrics were calculated for each bend of each river, the nine datasets were grouped according to their respective permafrost zones: Continuous Permafrost Bends (CPBs), Discontinuous Permafrost Bends (DPBs), and Non-Permafrost Bends (NPBs) (Table 5).

Table 5: Full dataset. The total number of half-meander bends in each of the three study groups.

Group	Bend Type			Total
	Simple	Two-Arc Compound	Discarded	
Continuous Permafrost Bends	121	88	39	248
Discontinuous Permafrost Bends	72	76	24	172
Non-Permafrost Bends	97	119	42	258
				678

CHAPTER V

RESULTS

To avoid performing statistical analyses on straight bends or bends with missing width data, the bends labeled as 'Discarded' were removed and a subset dataset of only simple and two-arc compounds was created (Table 6). Furthermore, even if not explicitly stated, all morphometric data used in the below statistical analyses are unitless and have been normalized where necessary. All statistical analyses were conducted in R version 4.1.1. Specific R packages, functions, and versions used, will be listed below.

Table 6: Subset dataset. The number of half-meander bends suitable for statistical analysis.

Group	Bend Type		Total
	Simple	Two-Arc Compound	
Continuous Permafrost Bends	121	88	209
Discontinuous Permafrost Bends	72	76	148
Non-Permafrost Bends	97	119	216
			573

Shapiro-Wilk Test

To assess the distributions of the bend variable datasets, a Shapiro-Wilk test of normality was conducted using the *shapiro.test* function from the R package *stats*. The test's null hypothesis is that a sample comes from a normally distributed population. The morphometrics tested were normalized bend length, sinuosity, normalized absolute average curvature, and asymmetry index (alpha level = 0.05) for each of the three bend groups. Only the simple and two-arc compound bends were used in this analysis, totaling 573 individual bends (Table 6). A

visual confirmation of the test results was conducted by visualizing the grouped distributions using the *ggdensity* function from the R package *ggpubr* v0.4.0. The results of the Shapiro-Wilk normality tests are in Table (7). The null hypothesis that the data comes from normally distributed populations was rejected for every morphometric across all three bend groups (alpha level = 0.05). Additionally, the distributions of every morphometric across all three bends was positively skewed (Figure 9).

Table 7: Results of the Shapiro Wilk normality test for simple and two-arc compound bends across three study groups.

Group	Morphometrics	P-Value	Normal Distribution
Continuous Permafrost Bends	Norm. Bend Length	9.883e-12	No: Positive Skew
	Sinuosity	2.415e-12	No: Positive Skew
	Norm. Abs. Avg. Curvature	5.456e-12	No: Positive Skew
	Asymmetry Index	0.0005632	No: Positive Skew
	Norm. Chord Length	7.657e-09	No: Positive Skew
Discontinuous Permafrost Bends	Norm. Bend Length	1.564e-06	No: Positive Skew
	Sinuosity	3.985e-10	No: Positive Skew
	Norm. Abs. Avg. Curvature	1.797e-12	No: Positive Skew
	Asymmetry Index	7.76e-05	No: Positive Skew
	Norm. Chord Length	0.01095	No: Positive Skew
Non-Permafrost Bends	Norm. Bend Length	2.885e-14	No: Positive Skew
	Sinuosity	1.204e-12	No: Positive Skew
	Norm. Abs. Avg. Curvature	9.15e-09	No: Positive Skew
	Asymmetry Index	1.867e-07	No: Positive Skew
	Norm. Chord Length	6.561e-11	No: Positive Skew

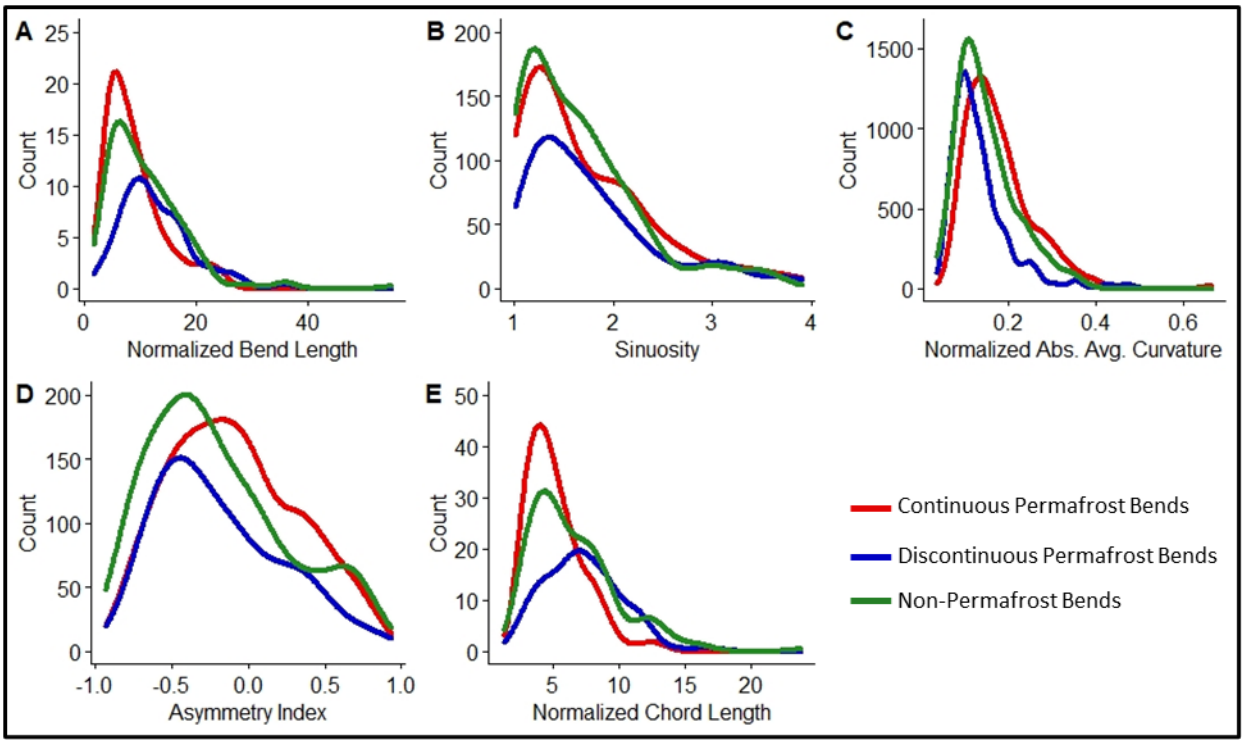

Figure 9: Distribution of bend morphometrics for Continuous Permafrost Bends (CPBs), Discontinuous Permafrost Bends (DPBs), and Non-Permafrost Bends (NPBs). Bend length and absolute average curvature were normalized with local average bend width.

Kolmogorov-Smirnov Test

To test if the morphometrics of rivers from different permafrost zones are statistically different from one another, a two-sided Kolmogorov-Smirnov test was conducted on the bend statistics using the *ks.test* function from the R package *stats*. The two-sided Kolmogorov-Smirnov test is a non-parametric test that compares the cumulative distribution functions of two sample distributions. The default null hypothesis is that the cumulative distributions of two samples are equal, and the default alternative hypothesis is that the distributions are not equal. However, the null hypothesis can be set to test whether the distribution of sample X is not less than or not greater than the distribution function of sample Y. Doing so provides more

information as to how the distribution of two samples differ. If the distribution of sample X is *greater* than the distribution of sample Y (i.e., above Y's), it is stochastically smaller than sample Y (Figure 10). This is critical in interpreting the distributions of the samples. The test reports a test statistic, D, which is the maximum difference between the two distributions, as well as the p-value associated with it. The p-value determines the statistical significance of that test-statistic, and whether the null hypothesis is rejected or not.

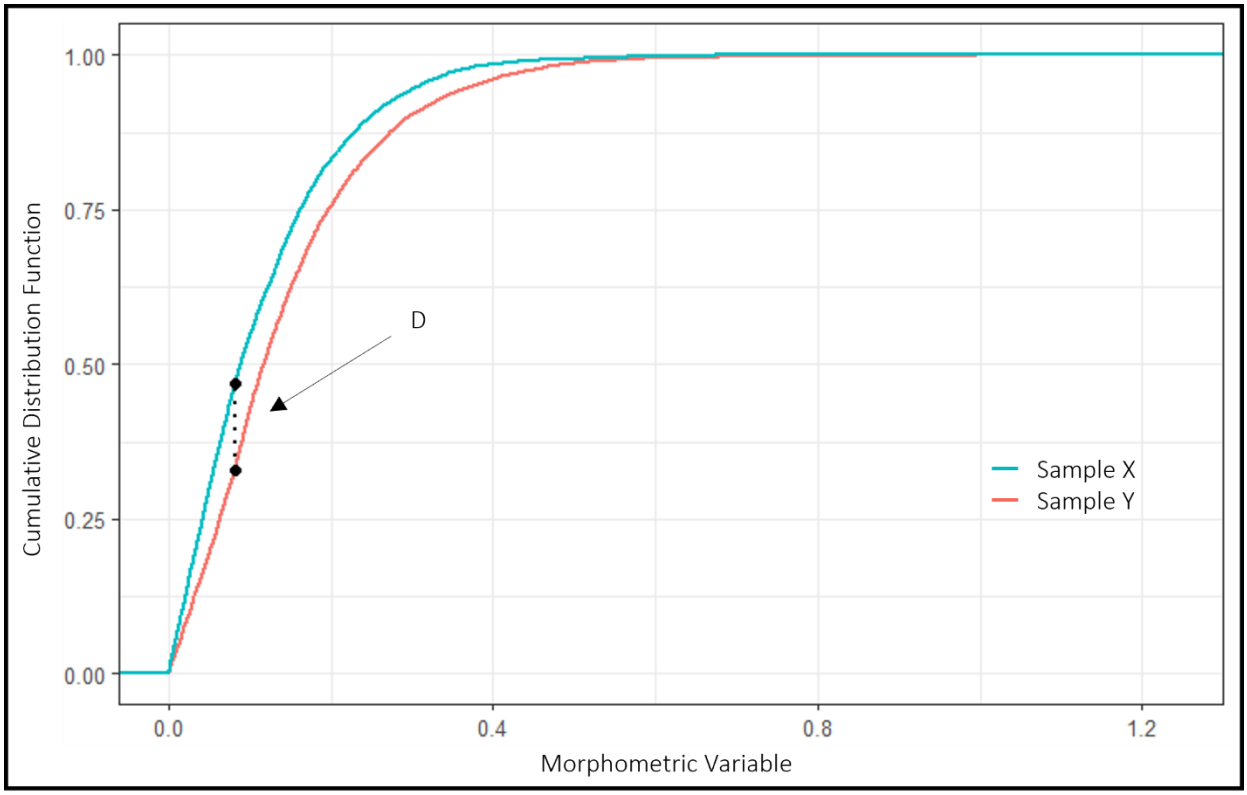

Figure 10: An example of what a Kolmogorov-Smirnov test analyzes. The test statistic, D, represents the maximum difference between two sample distributions and the associated p-value determines the significance of the test-statistic.

The morphometric variables tested were normalized bend and chord length, sinuosity, normalized absolute average curvature, and asymmetry index (alpha level = 0.05) for each of the

three bend groups. In other words, for every variable, CPBs vs. DPBs, CPBs vs. NPBs, and DPBs vs. NPBs was tested. Additionally, for each morphometric all three Kolmogorov-Smirnov scenarios were tested. To assess the impact of removing the bends labeled as 'Discarded' on the test results, Kolmogorov-Smirnov tests using both the complete dataset and the subset dataset were conducted.

Continuous Permafrost Bends vs. Discontinuous Permafrost Bends

The removal of bends labeled 'Discarded' did not result in any statistically significant changes to the Kolmogorov-Smirnov test results (Table 8). This was verified by comparing the p-value results from the two datasets and determining whether there was a change in the null hypothesis rejection.

Table 8: Kolmogorov-Smirnov test results between CPBs and DPBs on both the complete bends dataset and the subset dataset (only simple and two-arc compound bends). Significance level (a = 0.05) is constant.

Morphometric	Null Hyp. H_0	Alt. Hyp. H_1	Rejected Null Hyp.	P-Value (Full Dataset)	P-Value (Subset Data)
Norm. Bend Length	CPBs = DPBs	CPBs ≠ DPBs	Yes	5.501e-9	8.298e-9
	CPBs ≯ DPBs	CPBs > DPBs	Yes	2.750e-9	4.149e-9
	CPBs ≮ DPBs	CPBs < DPBs	No	1	1
Sinuosity	CPBs = DPBs	CPBs ≠ DPBs	No	0.1985	0.3172
	CPBs ≯ DPBs	CPBs > DPBs	No	0.0994	0.1593
	CPBs ≮ DPBs	CPBs < DPBs	No	0.7903	0.6891
Asymmetry Index	CPBs = DPBS	CPBs ≠ DPBs	Yes	0.0398	0.0205
	CPBs ≯ DPBs	CPBs > DPBs	No	0.9432	0.9689
	CPBs ≮ DPBs	CPBs < DPBs	Yes	0.0199	0.0103
Norm. Abs. Avg. Curvature	CPBs = DPBs	CPBs ≠ DPBs	Yes	8.852e-8	1.866e-8
	CPBs ≯ DPBs	CPBs > DPBs	No	0.9823	0.9869
	CPBs ≮ DPBs	CPBs < DPBs	Yes	4.426e-8	9.329e-9
Norm. Chord Length	CPBs = DPBs	CPBs ≠ DPBs	Yes	1.223e-12	5.272e-12
	CPBs ≯ DPBs	CPBs > DPBs	Yes	6.113e-13	2.636e-12
	CPBs ≮ DPBs	CPBs < DPBs	No	1	.9993

The cumulative distribution functions of half-meander sinuosity for the groups CPBs and DPBs were not found to be significantly different from one another. Bend length, asymmetry index, absolute average curvature, and chord length were significantly different from one another. In the bend and chord length tests, a p-value of below 0.05 confirmed a rejection of the null hypothesis that the CPBs and DPBs groups come from the same population. Testing for different scenarios showed that the cumulative distribution functions of CPBs bend and chord lengths lie above those of DPBs at a statistically significant distance. For asymmetry index and absolute average curvature, the null hypothesis was rejected that the cumulative distribution functions between the two groups is equal. Furthermore, testing for different scenarios showed that for these two morphometrics, the cumulative distribution function of CPBs lies below that of DPBs at a statistically significant distance.

It should be noted that a warning was returned during the Kolmogorov-Smirnov test for asymmetry index values of CPBs and DPBs. The test suffered from the presence of 'ties' in the two distributions. In other words, similar values were found in both groups, which impacts the exact significance (p-value) of the test statistic, D. To quantify the number of ties present, and whether removing the 'Discarded' bends helped reduce this number, I sorted the two datasets being tested and used the *duplicated* function in R to check for duplicates. A total of 55 and 33 ties were found in the full dataset and the subset dataset, respectively. In other words, removing the bends not suitable for half-meander analysis reduced the number of ties present in the group distributions by 22. It is unclear if the remaining 33 ties significantly alter the test results.

Continuous Permafrost Bends vs. Non-Permafrost Bends

The removal of bends labeled 'Discarded' did not result in any statistically significant changes to the Kolmogorov-Smirnov test results between CPBs and NPBs (Table 9). This was verified by comparing the p-value results from the two datasets and determining whether there was a change in the null hypothesis rejection.

Table 9: Kolmogorov-Smirnov test results between CPBs and NPBs on both the complete bends dataset and the subset dataset (only simple and two-arc compound bends). Significance level (a = 0.05) is constant.

Morphometric	Null Hyp. H_0	Alt. Hyp. H_1	Rejected Null Hyp.	P-Value (Full Dataset)	P-Value (Subset Data)
Norm. Bend Length	CPBs = NPBs	CPBs ≠ NPBs	Yes	0.0008	0.0067
	CPBs ≯ NPBs	CPBs > NPBs	Yes	0.0004	0.0033
	CPBs ≮ NPBs	CPBs < NPBs	No	0.9917	0.9911
Sinuosity	CPBs = NPBs	CPBs ≠ NPBs	No	0.4470	0.3639
	CPBs ≯ NPBs	CPBs > NPBs	No	0.5718	0.7607
	CPBs ≮ NPBs	CPBs < NPBs	No	0.2261	0.1830
Asymmetry Index	CPBs = NPBs	CPBs ≠ NPBs	Yes	0.0222	0.0091
	CPBs ≯ NPBs	CPBs > NPBs	No	0.9111	0.8267
	CPBs ≮ NPBs	CPBs < NPBs	Yes	0.0111	0.0045
Norm. Abs. Avg. Curvature	CPBs = NPBs	CPBs ≠ NPBs	Yes	0.0002	0.0005
	CPBs ≯ NPBs	CPBs > NPBs	No	0.9959	1
	CPBs ≮ NPBs	CPBs < NPBs	Yes	0.0001	0.0003
Norm. Chord Length	CPBs = NPBs	CPBs ≠ NPBs	Yes	5.804e-7	6.928e-5
	CPBs ≯ NPBs	CPBs > NPBs	Yes	2.902e-7	3.464e-5
	CPBs ≮ NPBs	CPBs < NPBs	No	1	0.9971

The cumulative distributions functions of sinuosity for the groups CPBs and NPBs were not found to be significantly different from one another. Bend length, asymmetry index, absolute average curvature, and chord length were significantly different from one another. In the bend length and chord length tests, a p-value of below 0.05 confirmed a rejection of the null

hypothesis that the CPBs and NPBs groups come from the same population. Testing for different scenarios showed that the cumulative distribution functions of CPBs bend and chord lengths lie above those of NPBs at a statistically significant distance. For asymmetry index and absolute average curvature, the null hypothesis was rejected that the cumulative distribution functions between the two groups is equal. Furthermore, testing for different scenarios showed that for these two morphometrics, the cumulative distribution function of CPBs lies below that of NPBs at a statistically significant distance. These results align with the results between the groups CPBs and DPBs across all morphometrics.

As with the results from the asymmetry index testing between CPBs and DPBs, a warning was returned during the Kolmogorov-Smirnov test for asymmetry index values of CPBs and NPBs. The tests also suffered from the presence of 'ties' in the two distributions. Again, I sorted the two datasets being tested and used the *duplicated* function in R to check for duplicates in the asymmetry index data of the two groups. A total of 36 and 19 ties were found in the full dataset and the subset dataset of the two groups, respectively. In other words, removing the bends not suitable for half-meander analysis reduced the number of ties present in the group distributions by 17. It is unclear if the remaining 19 ties significantly alter the test results.

Discontinuous Permafrost Bends vs. Non-Permafrost Bends

The removal of bends labeled 'Discarded' led to unexpected statistically significant changes to the Kolmogorov-Smirnov test results (Table 10). The unexpected change occurred in the testing of the morphometric sinuosity on the Kolmogorov-Smirnov test of DPBs $\not<$ NPBs. Using the entire dataset, the test result shows a significant difference between the two distributions (p-value = 0.0418), and I reject the null hypothesis that the distribution of DPBs is not less than the distribution function of NPBs. However, when the bends not suitable for

statistical analysis are removed, the p-value rises above 0.05 (p-value = 0.0903) and the null hypothesis cannot be rejected (a = 0.05). The change was unexpected because it is not supported by a significant result in the default test of DPBs = NPBs for sinuosity. Where, every previous significant morphometric tested has had one significant result in the default null hypothesis (X=Y) and one in the alternate scenarios tests (X$\succ$Y or X$\prec$Y).

Table 10: Kolmogorov-Smirnov test results between DPBs and NPBs on both the complete bends dataset and the subset dataset (only simple and two-arc compound bends). Significance level (a = 0.05) constant.

Morphometric	Null Hyp. H_0	Alt. Hyp. H_1	Rejected Null Hyp.	P-Value (Full Dataset)	P-Value (Subset Data)
Norm. Bend Length	DPBs = NPBs	DPBs ≠ NPBs	Yes	0.0038	0.0008
	DPBs $\succ$ NPBs	DPBs > NPBs	No	0.9808	0.9838
	DPBs $\prec$ NPBs	DPBs < NPBs	Yes	0.0019	0.0004
Sinuosity	DPBs = NPBs	DPBs ≠ NPBs	No	0.0836	0.1806
	DPBs $\succ$ NPBs	DPBs > NPBs	No	0.9391	1
	DPBs $\prec$ NPBs	DPBs < NPBs	Unclear	0.0418	0.0903
Asymmetry Index	DPBs = NPBs	DPBs ≠ NPBs	No	0.9558	0.7517
	DPBs $\succ$ NPBs	DPBs > NPBs	No	0.7104	0.5602
	DPBs $\prec$ NPBs	DPBs < NPBs	No	0.5921	0.4016
Norm. Abs. Avg. Curvature	DPBs = NPBs	DPBs ≠ NPBs	Likely	0.1227	0.0332
	DPBs $\succ$ NPBs	DPBs > NPBs	Likely	0.0614	0.0166
	DPBs $\prec$ NPBs	DPBs < NPBs	No	0.4299	0.8073
Norm. Chord Length	DPBs = NPBs	DPBs ≠ NPBs	Yes	0.0124	0.0030
	DPBs $\succ$ NPBs	DPBs > NPBs	No	0.2893	0.5447
	DPBs $\prec$ NPBs	DPBs < NPBs	Yes	0.0062	0.0015

An expected change in the results happened in the testing of the morphometric absolute average curvature on the Kolmogorov-Smirnov tests of DPBs = NPBs and DPBs $\succ$ NPBs. In both scenarios, removing the bends not suitable for analysis resulted in the distributions of DPBs and NPBs being significantly different from each other. I interpret this result as expected, based

on my belief that the bends not suitable for analysis distort signals of similarity or dissimilarity between true half-meander bends in the three groups, and thus should be removed. As well as that every previous significant morphometric tested has had one significant result in the default null hypothesis ($X=Y$) and one in the alternate scenarios tests ($X \succcurlyeq Y$ or $X \preccurlyeq Y$).

The cumulative distributions functions of asymmetry index for the groups DPBs and NPBs were not found to be significantly different from one another. Bend length distributions between the groups DPBs and NPBs were significantly different from one another. In the bend and chord length tests, a p-value of below 0.05 confirmed a rejection of the null hypothesis that the DPBs and NPBs groups come from the same population. Testing for different scenarios showed that the cumulative distribution functions of DPBs bend and chord lengths lie below those of NPBs at a statistically significant distance.

Principal Component Analysis

To determine if the bend morphometrics calculated in this study are suitable for the delineation of rivers in different permafrost zones, a principal component analysis (PCA) was conducted on the bend statistics using the *prcomp* function from the R package *stats*. A principal component analysis is a dimensionality-reduction method that projects data into new dimensions that represent the most variance in the dataset. In effect, it reduces the complexity of large datasets and highlights the potential underlying patterns among groups in the data along new dimensions (i.e., principal components) that represent the most variance in the dataset. In this case, reducing the dimensionality of the morphometrics into new fewer principal components that best highlight potential differences/similarities between the three bend groups. Interpretation of the PCA-transformed data is conducted using the reported variance of each new principal

component and a matrix of loadings relating the original morphometrics to the new principal components.

Prior to the PCA, the data were standardized through centering and scaling. In *prcomp,* centering is done by subtracting a variable's mean from each data point (bend value) and scaling by dividing each data point by a variable's standard deviation. If present, the standardization of data eliminates the influence of data range (scale) and unit differences. A lack of data standardization can result in faulty PCA results dominated by certain variables. In this analysis, scaling was critical to effectively compare normalized variables such as bend length and absolute average curvature, whose ranges differ in magnitude on an order of 4 (i.e., 2-55 vs. 0.0002-0.004).

Table 11: Importance of Principal Components

	Principal Component				
	PC1	PC2	PC3	PC4	PC5
Standard Deviation	1.5731	1.142	0.9312	0.56155	0.19436
Proportion of Variance	0.4949	0.261	0.1734	0.06307	0.00755
Cumulative Proportion	0.4949	0.756	0.9294	0.99245	1

A PCA was conducted on the normalized bend and chord length, normalized absolute average curvature, asymmetry index, and sinuosity of all simple and two-arc compound bends. The standard deviation, proportion of variance and cumulative proportion of the new principal components can be seen in Table 11 and are visually presented in Figure 11. The data on Figure 11 assists in the visual determination of how many principal components are required to explain most of the variation in the dataset. The first principal components represent approximately 50% of the proportion of variance in the data, and the first three principal components represent

approximately 93% of the proportion of variance in the dataset. Since the first three components represent the vast majority of the variance in the dataset, if we retain only those components the PCA has effectively reduced the dimension of the data from 5 to 3. To better understand the composition of these new principal components, a matrix of the loadings relating the metrics and the new dimensions can be analyzed (Table 12). The loadings on Table 12 show the correlation between the original morphometrics and the new principal components, with the higher the loading magnitude, the more a morphometric is represented or explained by a principal component.

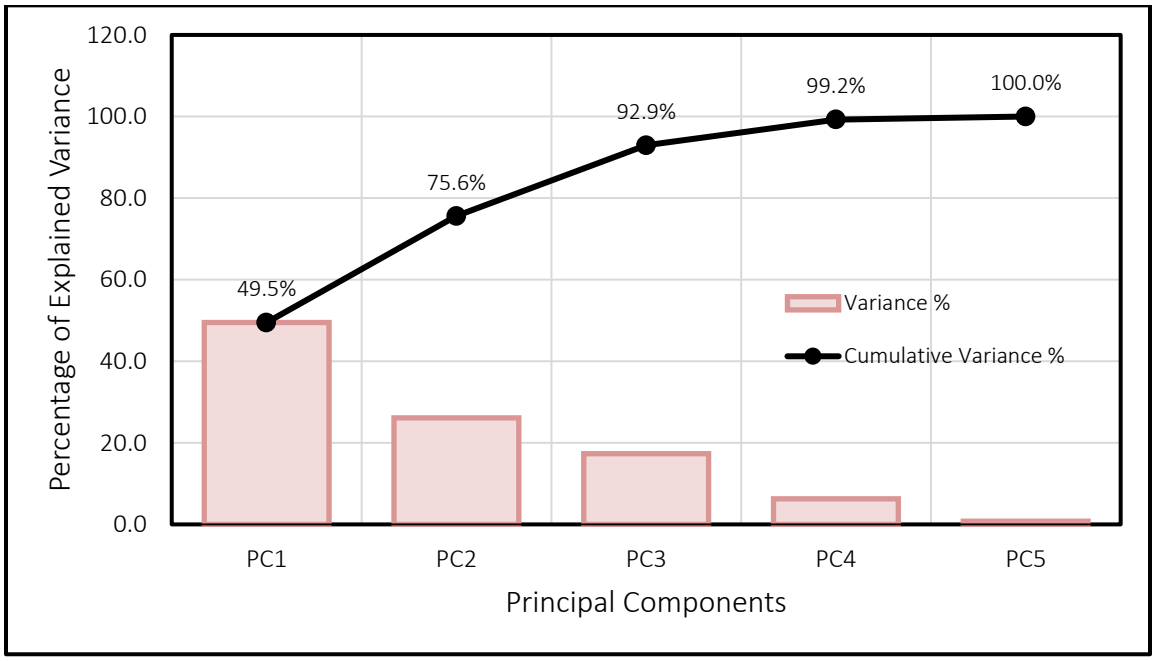

Figure 11: Plot of explained variance per principal component (PC#) and cumulative variance percentage.

Using these loadings and the *get_pca_var* function from the R package *factoextra,* the percent contributions of each morphometric for the first three principal components was calculated (Figure 12). Percent contributions is calculated as:

$$\%\ Contribution = \frac{loading^2 * 100}{total\ loadings^2} \qquad \textbf{Eq. 5}$$

where, *loading* represents a single loading of a variable on a principal component and *total loadings* represents all loadings of each variable on a principal component. For example, the contribution percentage of chord length on Principal Component 1 (PC1) is calculated as:

$$\%\ Contribution = \frac{0.881^2 * 100}{(0.881^2 + 0.929^2 + 0.355^2 + -0.286^2 + -0.792^2)}$$

Table 12: Principal Component and Morphometric Loadings.

	Principal Component				
	PC1	PC2	PC3	PC4	PC5
Norm. Chord Length	0.881	-0.361	0.050	0.279	-0.113
Norm. Bend Length	0.929	0.232	-0.196	0.165	0.135
Sinuosity	0.355	0.839	-0.381	-0.137	-0.083
Asymmetry Index	-0.286	-0.489	-0.824	0.016	0.000
Norm. Abs. Avg. Curvature	-0.792	0.423	-0.048	0.437	-0.005

As can be confirmed from the loadings on Table 12 and the percent contributions from Figure 12, higher loading magnitudes result in a higher percent contribution to a principal component. The dashed red line on Figure 12 represents the percent contribution mark if we assumed uniform contribution among the morphometrics (100% / # of metrics). I interpret any variable contributing more than 20% to a single component as significant. For PC1, bend length, chord length, and absolute average curvature all contribute significantly (Figure 12). Bend length

has the highest loading magnitude (0.929) and as a result is the highest contributor (34.8%) to it. Likewise, the morphometric asymmetry index has the lowest loading magnitude (-0.286) and has the lowest contribution (3.3%) to PC1. PC2 only has one significant contributor in the morphometric sinuosity at 53.9%. Asymmetry index is a close significant contributor at 18.3%. PC3 also only has one significant contributor in asymmetry index at 78.3%.

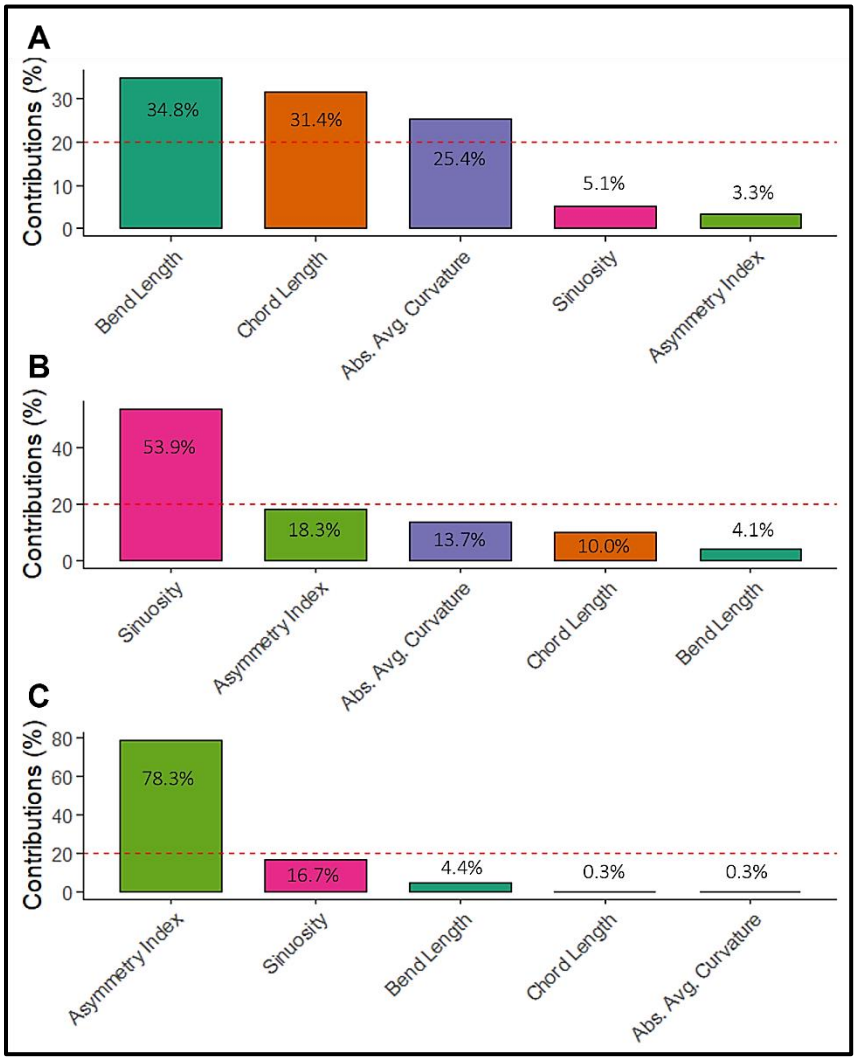

Figure 12: Morphometrics' contribution percentages for the first three principal components. A) Principal Component 1. B) Principal Component 2. C) Principal Component 3.

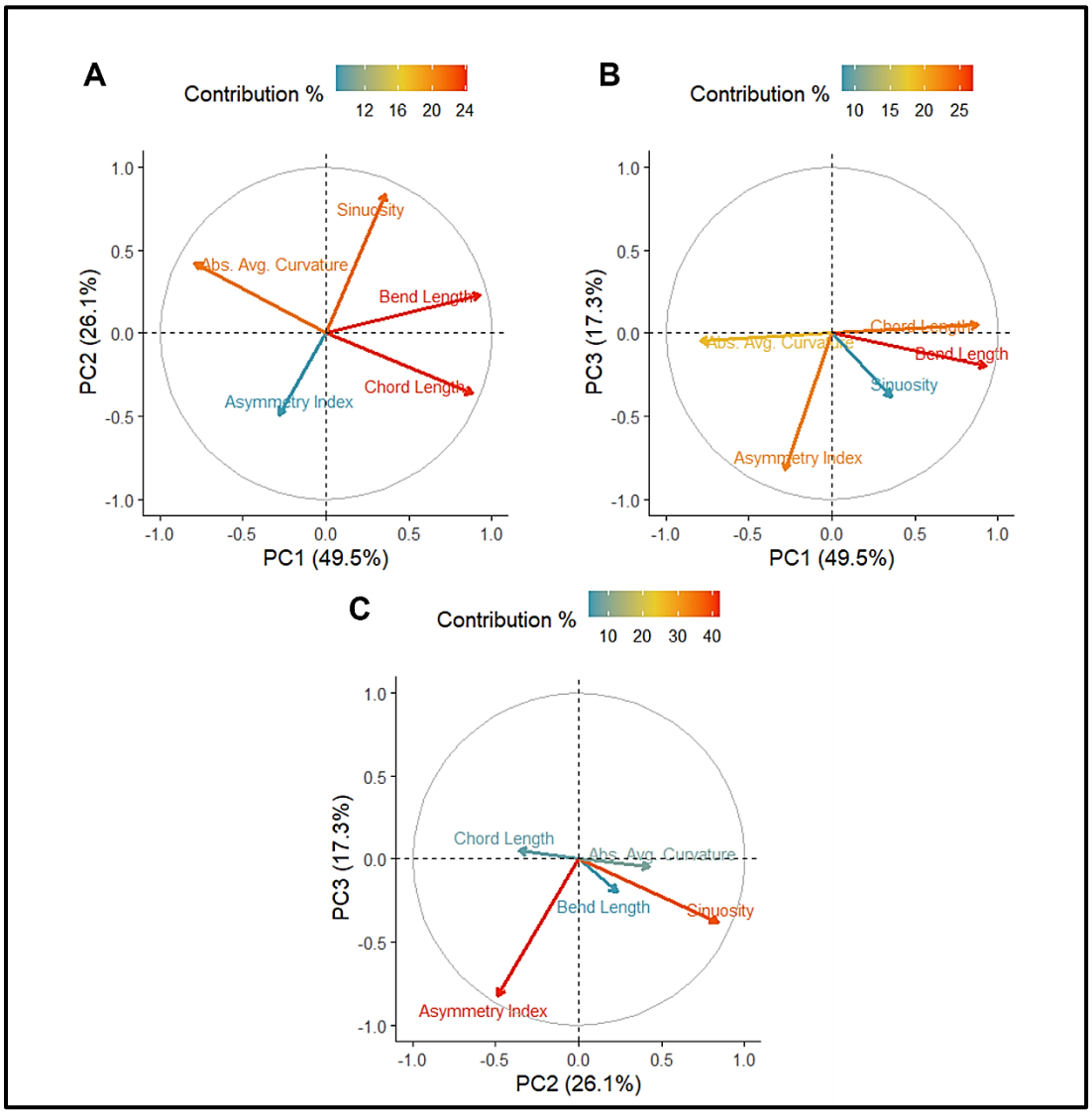

Figure 13: Morphometrics visualized according to their percent contribution to a 2D principal component space. A) Principal components 1 and 2. B) Principal components 1 and 3. C) Principal components 2 and 3.

The contributions of each morphometric were also visualized in 2-dimensions (Figure 13). Each subplot in Figure 13 represents the percent contribution of each morphometric between two principal components. Each morphometric variable is represented by a vector, the closer a

morphometric vector is to the correlation circle, the more it is correlated with the principal component along the nearest axis, and the shorter and farther it is from the circle's edge, the less correlated it is with the corresponding principal component axis. These two-dimensional plots assist in better understanding the spread of data across the components that best represent the variance in the original subset dataset. Since PC1 and PC2 combine for 75.6% of the variance, Figure 13-A is the primary focus. Collectively, the morphometrics bend length, chord-length, sinuosity, and absolute average curvature are well correlated with the two-dimensional space created by PC1 and PC2. For the space created by PC1 and PC3, the same applies except asymmetry index is now well represented along the PC3 axis and sinuosity is not well represented by either dimension. Lastly, only asymmetry index and sinuosity are well represented by the two-dimensional space created by PC2 and PC3.

The morphometric vectors were plotted with the PCA transformed individual bend data in 2D plots for the first three principal components (Figure 14). The transformed bend data is color-coded according to the three study groups and confidence ellipses (95%) are drawn to highlight group clustering areas. Although PCA is not intentionally a cluster delineation method, plotting the results can visually highlight differences in the data, and thus highlight the clustering of groups. It is clear from all three combinations of retained principal components (1-3) that there is no visible delineation between the cluster area of the study groups.

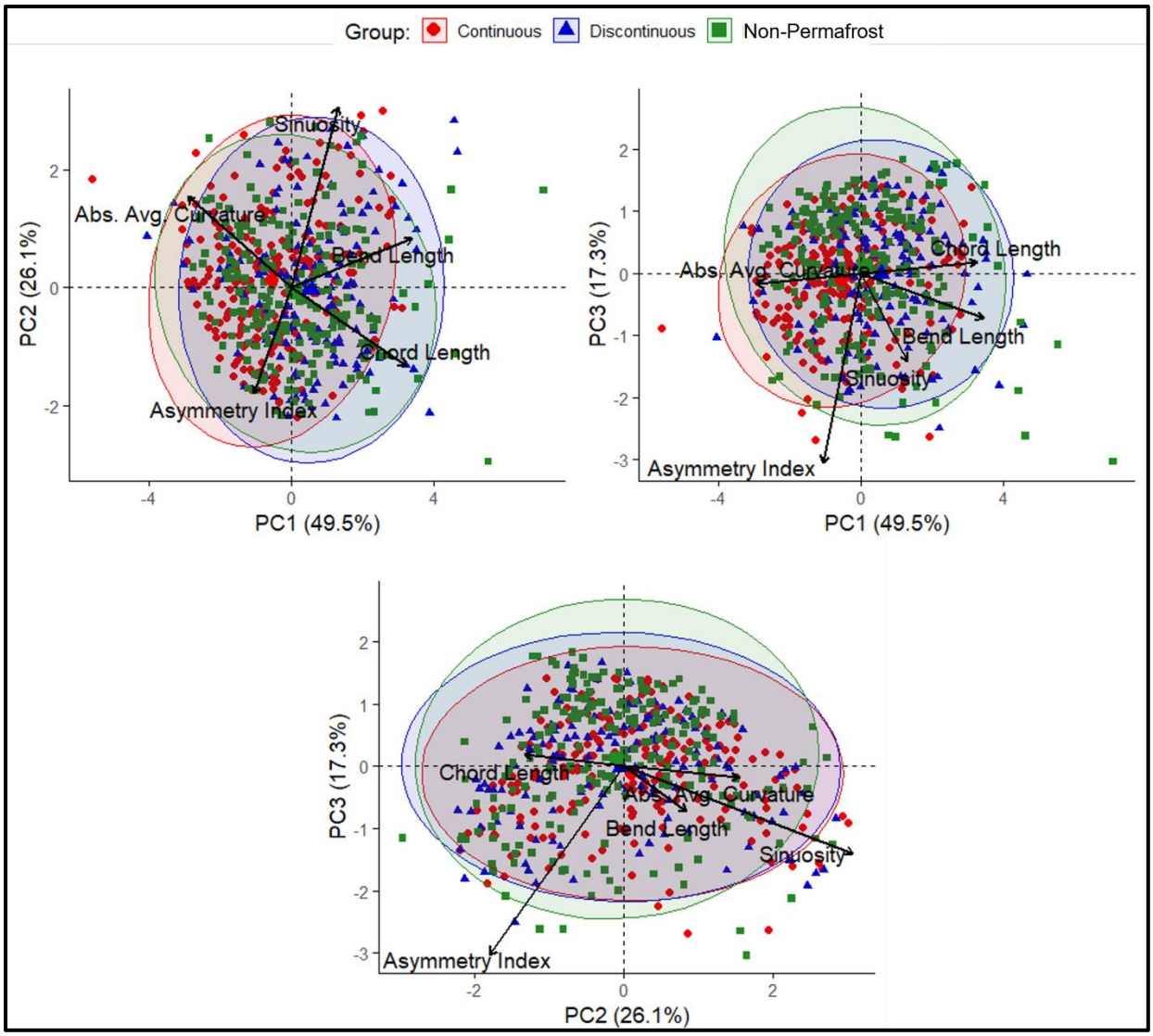

Figure 14: Combination plots of morphometric variable vectors and transformed bend data per study group between PCs 1-3.

CHAPTER VI

DISCUSSION AND CONCLUSION

Summary and Interpretation of Results

A subset dataset of 573 bends was statistically analyzed to determine if the morphometrics of river bends in different permafrost zones (Continuous Permafrost, Discontinuous Permafrost, and Non-Permafrost) are statistically different from one another and if the generated set of morphometrics alone is enough to delineate between bends in different zones. A Shapiro-Wilk test of normality was conducted on each morphometric across the three study groups and the null hypothesis that the data come from normally distributed populations was rejected for every single one (alpha level = 0.05). A visual confirmation of the results further showed that all 15 individual distributions (5 morphometrics * 3 study groups) are positively skewed. Meaning that most of the data can be represented by relatively smaller values and a few bends are represented by high extremes. Similar distributions are seen in Finotello et al. (2020).

The results of multiple Kolmogorov-Smirnov tests comparing the three bend groups across five select morphometrics, indicate that CPBs are morphometrically different from DPBs and NPBS across all bend morphometrics calculated, except for sinuosity. These differences align with the hypothesis that permafrost plays a critical role in the evolution of Arctic rivers, where the largest differences in the morphology of river bends will be between those found in areas with the highest areal extent of permafrost and those with less or none at all. Furthermore, the relationships of the cumulative distribution functions between CPBs and both DPBS and NPBs are the same for the morphometrics bend length, asymmetry index, absolute average curvature, and chord length. In other words, the exact same Kolmogorov-Smirnov tests and

alternative hypothesis scenarios that returned as statistically significant for CPBs vs. DPBs, returned as statistically significant for CPBs vs. NPBs. For example, at statistically significant levels (alpha level = 0.05) the bend length distribution curves for CPBs were above those of DPBs and NPBs. Meaning that the CPBs data is stochastically smaller than the DPBs and NPBs bend length data. This is confirmed by calculating the bend length distribution statistics for each of the three groups and comparing them (Table 13).

Table 13: Summary statistics for each morphometric distribution. All values are unitless via normalization or by default.

	Summary Statistics						
	Group	Minimum	1st Quartile	Median	Mean	3rd Quartile	Maximum
Bend Length	CPBs	1.761	5.246	7.718	9.139	11.376	26.033
	DPBs	2.833	8.343	11.612	12.851	16.403	36.152
	NPBs	2.334	5.886	9.377	11.006	14.297	54.998
Asymmetry Index	CPBs	-0.854	-0.429	-0.111	-0.089	0.250	0.846
	DPBs	-0.933	-0.500	-0.276	-0.188	0.083	0.907
	NPBs	-0.897	-0.538	-0.286	-0.190	0.074	0.938
Absolute Average Curvature	CPBs	0.066	0.123	0.159	0.177	0.212	0.665
	DPBs	0.056	0.090	0.116	0.134	0.152	0.469
	NPBs	0.036	0.101	0.134	0.149	0.184	0.375
Chord Length	CPBs	1.334	3.636	4.736	5.218	6.306	13.636
	DPBs	1.966	5.243	7.023	7.304	9.113	17.256
	NPBs	2.255	4.135	5.731	6.619	8.331	23.803
Sinuosity	CPBs	1.017	1.198	1.499	1.74	2.108	3.898
	DPBs	1.038	1.284	1.626	1.801	2.089	3.891
	NPBs	1.022	1.195	1.553	1.671	1.945	3.703

Cross-referencing the Kolmogorov-Smirnov test results with the summary statistics from Table 13 confirms that when compared to DPBs and NPBs, CPBs are 1) smaller in size (via chord and bend length), 2) have a lower chance of being upstream skewed (via asymmetry index)

and 3) on average have sharper bends and sharp transition zones between bends (via absolute average curvature). However, the thematic differences between DPBs and NPBs are less clear. DPBs are larger in size but have less-sharp planforms, and there is no statistically significant difference between their orientations (asymmetry index). Furthermore, the Kolmogorov-Smirnov results for sinuosity indicate no statistically significant differences in their distributions, except for a strange result wherein removing the 'Discarded' bends from analysis made the distance between cumulative distributions change from significant to insignificant. This change in significance is likely because several of the discarded bends are straight portions of the reach where sinuosity approximates 1 (bend length ≈ chord length). A removal of such a significant outlier could be why the distributions are not significantly different from one another according to a Kolmogorov-Smirnov test.

The results of the PCA on the combined morphometrics showed that the first three principal components account for 92.9% of the variance in the subset dataset of only simple and two-arc compound bends. The results indicate that Principal Component 1 is driving most of the variation in the data at 49.5%. Principal Component 1 is most representative of bend length, chord length, and absolute average curvature. In other words, the first principal component best represents the size and shape of half-meander bends. Principal Components 2 and 3 are only representative of one morphometric each, sinuosity and asymmetry index, respectively. Since they are only representative of one morphometric variable each, they provide no practical use in the reduction of dimensionality in the dataset.

The plotting of PCA transformed data indicated that while the individual morphometrics are useful in differentiating the characteristics of half-meander bends in different permafrost zones, when combined in a PCA there is no visible delineation between cluster areas of the three

study groups (Figure 13). This pattern is evident across all three combinations of retained principal components (1-3). This is perhaps counter intuitive: how can the bends be different on an individual morphometric basis but not when those metrics are combined? Some possible explanations of this are: 1) incorrect pre-processing of river planform data, 2) an inappropriate riverine scale, 3) inadequate morphometrics for Arctic river morphological characterization, and 4) areal extent of permafrost alone is not enough to differentiate between potentially different Arctic meandering river bend types.

It is possible that in an attempt to remove digitizing artifacts and inconsistencies through a Savitzky-Golay Filter and then a centerline resampling procedure, the true geomorphic signal of the centerline was lost. A qualitative re-analysis of the original and final centerlines showed that the final river centerlines were often slightly shifted inward towards the point bar of a bend. This slight shift could have impacted each of the morphometrics. As a result, future studies should investigate the sensitivity of morphometrics to different centerline generation methods, particularly if the margin between bends from different permafrost zones is small, but present.

The riverine scale of this analysis was conducted at the half-meander bend scale; however, it is possible that to unearth the morphodynamics signature differences between Arctic rivers, this type of analysis needs to be conducted at a reach-scale. In other words, while there are differences statically at a bend scale, a reach-scale analysis could lead to clear delineation between rivers from different permafrost zones in a PCA. At a reach-scale the values for each morphometric would represent a morphological trait of an entire section of river, instead of just one individual half-meander bend. Previous studies have found success delineating between different rivers by performing morphometric analyses at a reach-scale (Howard and Hemberger 1991; Finotello et al. 2020; Frascati and Lanzoni 2009).

It is possible that the morphometrics selected for this analysis are not the best metrics to characterize the morphological characteristics of high-latitude permafrost rivers. There is no definitive way to determine which morphometrics should be used in a morphodynamics analysis of rivers. While there are standard measurements of bend units, such as the ones used here, there exists a wide variety of morphometrics for different riverine scales. Furthermore, it can be argued that while the five morphometrics used here are useful in identifying differences at a bend-scale, to differentiate between different Arctic River forms, more complex morphometrics that capture more variety in a bends shape, orientation, and size are required. It might prove insightful to attempt this same analysis with a combination of half-meander metrics, full-meander metrics, and reach-scale metrics, as defined in Howard and Hemberger (1991).

Lastly, the areal extent of permafrost might not be enough to differentiate between potentially different Arctic meandering river bend types. While one of the goals of this study was to determine if the areal extent of permafrost alone was enough to differentiate between different bend morphologies, it would be inaccurate to assume that this alone is the controlling factor on the evolution of Arctic river bends. I recommend that future studies assess other potentially contributing floodplain factors such as hydrology (i.e., discharge volumes, timing of flow, etc.), watershed size, the role of river-ice on bend evolution, mean water temperatures as it relates to riverbank permafrost degradation, and local permafrost characteristics (e.g., ice percent, active layer depth, reach-scale permafrost heterogeneity).

Conclusions

A morphometric analysis using the bend and chord length, sinuosity, absolute average curvature, and asymmetry index of approximately 600 Arctic and sub-Arctic river bends indicates that bends from the continuous permafrost zones, discontinuous permafrost zones, and

high-latitude non-permafrost regions are morphometrically different from one another at a half-meander bend scale. More specifically, results indicate that bends from the continuous permafrost zone, when compared to other bends from Arctic or sub-Arctic rivers, are statistically more likely to be 1) smaller in size (via chord and bend length), 2) have a lower chance of being upstream skewed (via asymmetry index) and 3) on average have sharper bends and sharp transition zones between bends (via absolute average curvature). However, the combination of the half-meander bend morphometrics when transformed via PCA, are alone not enough to delineate between river bends of different permafrost zones. Some possible explanations of this are: 1) incorrect pre-processing of river planform data 2) an inappropriate riverine scale 3) inadequate morphometrics for Arctic river morphological characterization 4) areal permafrost extent alone is not enough to differentiate between potentially different Arctic meandering river bend types.

To answer any of these questions, more analyses on the morphological characteristics of Arctic rivers is required. I propose that future investigation into the characterization of rivers in permafrost environments focus not only on generalized areal permafrost extents, but on factors such as hydrology (i.e., discharge volumes, timing of flow, etc.), watershed size, the role of river-ice on bend evolution, mean water temperatures as it relates to riverbank permafrost degradation, and local permafrost characteristics (e.g., ice percent, active layer depth, reach-scale permafrost heterogeneity).

As previously highlighted by Lininger and Wohl (2019), Arctic riverine environments will no longer be the static environments they were once characterized as. As both drivers and indicators of climatic changes, Arctic rivers will continue to be an important factor in pan-Arctic feedback systems. Although this study successfully delineated Arctic river planforms, quantified

the morphological characteristics of their half-meander bends, and showed that statistically significant differences exist between bends from different permafrost zones, there is a significant lack of fundamental understanding on how river morphology interacts and is shaped by floodplain permafrost.

The Arctic is changing drastically and understanding the feedback processes between permafrost degradation and river evolution will become increasingly critical. This form of analysis on bend and reach characteristics of Arctic rivers should be conducted regularly to monitor the changes in the form and shape of rivers across not only permafrost characteristics but other drivers of floodplain dynamics. Doing so will reveal the resistance of existing Arctic river morphology to climatic changes in the floodplain, and hopefully provide insight into potential geomorphic tipping points, where a shift in the form, shape, and evolution of permafrost-region rivers occurs.

REFERENCES

Alfredsen, Knut. 2017. "An Assessment of Ice Effects on Indices for Hydrological Alteration in Flow Regimes." *Water* 9 (12): 914. https://www.mdpi.com/2073-4441/9/12/914.

Allen, George H., and Tamlin M. Pavelsky. 2015. "Patterns of river width and surface area revealed by the satellite-derived North American River Width data set." *Geophysical Research Letters* 42 (2): 395-402. https://doi.org/https://doi.org/10.1002/2014GL062764. https://agupubs.onlinelibrary.wiley.com/doi/abs/10.1002/2014GL062764.

---. 2018. "Global extent of rivers and streams." *Science* 361 (6402): 585-588. https://doi.org/10.1126/science.aat0636. https://science.sciencemag.org/content/sci/361/6402/585.full.pdf.

Arzhanov, M. M., A. V. Eliseev, and I. I. Mokhov. 2013. "Impact of climate changes over the extratropical land on permafrost dynamics under RCP scenarios in the 21st century as simulated by the IAP RAS climate model." *Russian Meteorology and Hydrology* 38 (7): 456-464. https://doi.org/10.3103/S1068373913070030. https://doi.org/10.3103/S1068373913070030.

Ballinger, T. J., J. E. Overland, M. Wang, U. S. Bhatt, E. Hanna, I. Hanssen-Bauer, S. J. Kim, R. L. Thoman, and J. E. Walsh. 2020. "Arctic Report Card 2020: Surface Air Temperature." https://doi.org/https://doi.org/10.25923/gcw8-2z06. https://repository.library.noaa.gov/view/noaa/27901.

Beck, Hylke E., Niklaus E. Zimmermann, Tim R. McVicar, Noemi Vergopolan, Alexis Berg, and Eric F. Wood. 2018. "Present and future Köppen-Geiger climate classification maps at 1-km resolution." *Scientific Data* 5 (1): 180214. https://doi.org/10.1038/sdata.2018.214. https://doi.org/10.1038/sdata.2018.214.

Bennett, K. E., and T. D. Prowse. 2010. "Northern Hemisphere geography of ice-covered rivers." *Hydrological Processes* 24 (2): 235-240. https://doi.org/https://doi.org/10.1002/hyp.7561. https://onlinelibrary.wiley.com/doi/abs/10.1002/hyp.7561.

Bhatt, Uma S., Donald A. Walker, Martha K. Raynolds, Josefino C. Comiso, Howard E. Epstein, Gensuo Jia, Rudiger Gens, Jorge E. Pinzon, Compton J. Tucker, Craig E. Tweedie, and Patrick J. Webber. 2010. "Circumpolar Arctic Tundra Vegetation Change Is Linked to

Sea Ice Decline." *Earth Interactions* 14 (8): 1-20. https://doi.org/10.1175/2010ei315.1. https://journals.ametsoc.org/view/journals/eint/14/8/2010ei315.1.xml.

Bintanja, R. 2018. "The impact of Arctic warming on increased rainfall." *Scientific Reports* 8 (1): 16001. https://doi.org/10.1038/s41598-018-34450-3. https://doi.org/10.1038/s41598-018-34450-3.

Bintanja, R., and O. Andry. 2017. "Towards a rain-dominated Arctic." *Nature Climate Change* 7 (4): 263-267. https://doi.org/10.1038/nclimate3240. https://doi.org/10.1038/nclimate3240.

Bintanja, R., and F. M. Selten. 2014. "Future increases in Arctic precipitation linked to local evaporation and sea-ice retreat." *Nature* 509 (7501): 479-482. https://doi.org/10.1038/nature13259. https://doi.org/10.1038/nature13259.

Biskaborn, B. K., S. L. Smith, J. Noetzli, H. Matthes, G. Vieira, D. A. Streletskiy, P. Schoeneich, V. E. Romanovsky, A. G. Lewkowicz, A. Abramov, M. Allard, J. Boike, W. L. Cable, H. H. Christiansen, R. Delaloye, B. Diekmann, D. Drozdov, B. Etzelmuller, G. Grosse, M. Guglielmin, T. Ingeman-Nielsen, K. Isaksen, M. Ishikawa, M. Johansson, H. Johannsson, A. Joo, D. Kaverin, A. Kholodov, P. Konstantinov, T. Kroger, C. Lambiel, J. P. Lanckman, D. L. Luo, G. Malkova, I. Meiklejohn, N. Moskalenko, M. Oliva, M. Phillips, M. Ramos, A. B. K. Sannel, D. Sergeev, C. Seybold, P. Skryabin, A. Vasiliev, Q. B. Wu, K. Yoshikawa, M. Zheleznyak, and H. Lantuit. 2019. "Permafrost is warming at a global scale." *Nature Communications* 10: 11. https://doi.org/10.1038/s41467-018-08240-4. <Go to ISI>://WOS:000455762900008.

Bjorkman, Anne D., Mariana García Criado, Isla H. Myers-Smith, Virve Ravolainen, Ingibjörg Svala Jónsdóttir, Kristine Bakke Westergaard, James P. Lawler, Mora Aronsson, Bruce Bennett, Hans Gardfjell, Starri Heiðmarsson, Laerke Stewart, and Signe Normand. 2020. "Status and trends in Arctic vegetation: Evidence from experimental warming and long-term monitoring." *Ambio* 49 (3): 678-692. https://doi.org/10.1007/s13280-019-01161-6. https://doi.org/10.1007/s13280-019-01161-6.

Brice, James C. 1974. "Evolution of Meander Loops." *GSA Bulletin* 85 (4): 581-586. https://doi.org/10.1130/0016-7606(1974)85<581:Eoml>2.0.Co;2. https://doi.org/10.1130/0016-7606(1974)85<581:EOML>2.0.CO;2.

Brooks, Rheannon N., Terry D. Prowse, and Ian J. O'Connell. 2013. "Quantifying Northern Hemisphere freshwater ice." *Geophysical Research Letters* 40 (6): 1128-1131.

https://doi.org/https://doi.org/10.1002/grl.50238. https://agupubs.onlinelibrary.wiley.com/doi/abs/10.1002/grl.50238.

Brown, J., O. J. Ferrians Jr, J. A. Heginbottom, and E. S. Melnikov. 1997. *Circum-Arctic map of permafrost and ground-ice conditions.* http://pubs.er.usgs.gov/publication/cp45.

Brown, J., O. Ferrians, J. A. Heginbottom, and E. Melnikov. 2002. Circum-Arctic Map of Permafrost and Ground-Ice Conditions Version 2. Boulder, Colorado USA: NSIDC: National Snow and Ice Data Center. https://doi.org/10.7265/skbgkf16.

Castillo, Cesar R., İnci Güneralp, Billy Hales, and Burak Güneralp. 2020. "Scale-Free Structure of Surface-Water Connectivity Within a Lowland River-Floodplain Landscape." *Geophysical Research Letters* 47 (16): e2020GL088378. https://doi.org/https://doi.org/10.1029/2020GL088378. https://agupubs.onlinelibrary.wiley.com/doi/abs/10.1029/2020GL088378.

Cavalieri, D. J., and C. L. Parkinson. 2012. "Arctic sea ice variability and trends, 1979–2010." *The Cryosphere* 6 (4): 881-889. https://doi.org/10.5194/tc-6-881-2012. https://tc.copernicus.org/articles/6/881/2012/.

Costard, F., L. Dupeyrat, E. Gautier, and E. Carey-Gailhardis. 2003. "Fluvial thermal erosion investigations along a rapidly eroding river bank: application to the Lena River (central Siberia)." *Earth Surface Processes and Landforms* 28 (12): 1349-1359. https://doi.org/https://doi.org/10.1002/esp.592. https://onlinelibrary.wiley.com/doi/abs/10.1002/esp.592.

Costard, François, E. Gautier, A. Fedorov, P. Konstantinov, and L. Dupeyrat. 2014. "An Assessment of the Erosion Potential of the Fluvial Thermal Process during Ice Breakups of the Lena River (Siberia)." *Permafrost and Periglacial Processes* 25 (3): 162-171. https://doi.org/https://doi.org/10.1002/ppp.1812. https://onlinelibrary.wiley.com/doi/abs/10.1002/ppp.1812.

Dai, Aiguo, and Kevin E. Trenberth. 2002. "Estimates of Freshwater Discharge from Continents: Latitudinal and Seasonal Variations." *Journal of Hydrometeorology* 3 (6): 660-687. https://doi.org/10.1175/1525-7541(2002)003<0660:Eofdfc>2.0.Co;2. https://journals.ametsoc.org/view/journals/hydr/3/6/1525-7541_2002_003_0660_eofdfc_2_0_co_2.xml.

Dean, K. G., W. J. Stringer, K. Ahlnäs, C. Searcy, and T. Weingartner. 1994. "The influence of river discharge on the thawing of sea ice, Mackenzie River Delta: albedo and temperature analyses." *Polar Research* 13 (1): 83-94. https://doi.org/10.3402/polar.v13i1.6683. https://doi.org/10.3402/polar.v13i1.6683.

Epstein, Howard E, Isla Myers-Smith, and Donald A Walker. 2013. "Recent dynamics of arctic and sub-arctic vegetation." *Environmental Research Letters* 8 (1): 015040.

Fagherazzi, Sergio, Emmanuel J. Gabet, and David Jon Furbish. 2004. "The effect of bidirectional flow on tidal channel planforms." *Earth Surface Processes and Landforms* 29 (3): 295-309. https://doi.org/https://doi.org/10.1002/esp.1016. https://onlinelibrary.wiley.com/doi/abs/10.1002/esp.1016.

FAO, IIASA, ISRIC, ISSCAS, and JRC. 2012. "Harmonized World Soil Database (version 1.2)." FAO, Rome, Italy and IIASA, Laxenburg, Austria.

Finotello, Alvise, Andrea D'Alpaos, Manuel Bogoni, Massimiliano Ghinassi, and Stefano Lanzoni. 2020. "Remotely-sensed planform morphologies reveal fluvial and tidal nature of meandering channels." *Scientific Reports* 10 (1): 54. https://doi.org/10.1038/s41598-019-56992-w. https://doi.org/10.1038/s41598-019-56992-w.

Fisher, G. Burch, Bodo Bookhagen, and Colin B. Amos. 2013. "Channel planform geometry and slopes from freely available high-spatial resolution imagery and DEM fusion: Implications for channel width scalings, erosion proxies, and fluvial signatures in tectonically active landscapes." *Geomorphology* 194: 46-56. https://doi.org/https://doi.org/10.1016/j.geomorph.2013.04.011. https://www.sciencedirect.com/science/article/pii/S0169555X13002171.

Frascati, Alessandro, and Stefano Lanzoni. 2009. "Morphodynamic regime and long-term evolution of meandering rivers." *Journal of Geophysical Research: Earth Surface* 114 (F2). https://doi.org/https://doi.org/10.1029/2008JF001101. https://agupubs.onlinelibrary.wiley.com/doi/abs/10.1029/2008JF001101.

Frasson, Renato Prata de Moraes, Tamlin M. Pavelsky, Mark A. Fonstad, Michael T. Durand, George H. Allen, Guy Schumann, Christine Lion, R. Edward Beighley, and Xiao Yang. 2019. "Global Relationships Between River Width, Slope, Catchment Area, Meander Wavelength, Sinuosity, and Discharge." *Geophysical Research Letters* 46 (6): 3252-3262. https://doi.org/https://doi.org/10.1029/2019GL082027. https://agupubs.onlinelibrary.wiley.com/doi/abs/10.1029/2019GL082027.

Frey, Karen E., and James W. McClelland. 2009. "Impacts of permafrost degradation on arctic river biogeochemistry." *Hydrological Processes: An International Journal* 23 (1): 169-182.

Frothingham, Kelly M., and Bruce L. Rhoads. 2003. "Three-dimensional flow structure and channel change in an asymmetrical compound meander loop, Embarras River, Illinois." *Earth Surface Processes and Landforms* 28 (6): 625-644. https://doi.org/https://doi.org/10.1002/esp.471. https://onlinelibrary.wiley.com/doi/abs/10.1002/esp.471.

Fuchs, Matthias, Ingmar Nitze, Jens Strauss, Frank Günther, Sebastian Wetterich, Alexander Kizyakov, Michael Fritz, Thomas Opel, Mikhail N Grigoriev, and Georgy T Maksimov. 2020. "Rapid fluvio-thermal erosion of a yedoma permafrost cliff in the Lena River Delta." *Frontiers in Earth Science* 8 (336).

GISTEMP-Team. 2022. GISS Surface Temperature Analysis (GISTEMP), version 4. NASA Goddard Institute for Space Studies. Dataset accessed 2022-02-05 at https://data.giss.nasa.gov/gistemp/.

Güneralp, İnci, Anthony M. Filippi, and Billy Hales. 2014. "Influence of river channel morphology and bank characteristics on water surface boundary delineation using high-resolution passive remote sensing and template matching." *Earth Surface Processes and Landforms* 39 (7): 977-986.

Haine, Thomas W. N., Beth Curry, Rüdiger Gerdes, Edmond Hansen, Michael Karcher, Craig Lee, Bert Rudels, Gunnar Spreen, Laura de Steur, Kial D. Stewart, and Rebecca Woodgate. 2015. "Arctic freshwater export: Status, mechanisms, and prospects." *Global and Planetary Change* 125: 13-35. https://doi.org/https://doi.org/10.1016/j.gloplacha.2014.11.013. https://www.sciencedirect.com/science/article/pii/S0921818114003129.

Hamming, Richard Wesley. 1983. *Digital filters*. New Jersey: Prentice-Hall.

Harris, S. A., H. M. French, J. A. Heginbottom, G. H. Johnston, B. Ladanyi, D. C. Sego, and R. O. van Everdingen. 1988 1988. *Glossary of permafrost and related ground-ice terms.* National Research Council of Canada. Associate Committee on Geotechnical Research. Permafrost Subcommittee.

Heather, Best, P. McNamara James, and Liberty Lee. 2005. "Association of Ice and River Channel Morphology Determined Using Ground-Penetrating Radar in the Kuparuk River, Alaska." *Arctic, Antarctic, and Alpine Research* 37 (2): 157-162. http://www.jstor.org/stable/4139073.

Heginbottom, J. Alan. 2002. "Permafrost mapping: a review." *Progress in Physical Geography: Earth and Environment* 26 (4): 623-642. https://doi.org/10.1191/0309133302pp355ra. https://journals.sagepub.com/doi/abs/10.1191/0309133302pp355ra.

Heginbottom, JA, J Brown, ES Melnikov, and OJ Ferrians Jr. 1993. "Circumarctic map of permafrost and ground ice conditions." Proceedings of the Sixth International Conference on Permafrost.

Hjort, Jan, Olli Karjalainen, Juha Aalto, Sebastian Westermann, Vladimir E. Romanovsky, Frederick E. Nelson, Bernd Etzelmüller, and Miska Luoto. 2018. "Degrading permafrost puts Arctic infrastructure at risk by mid-century." *Nature Communications* 9 (1): 5147. https://doi.org/10.1038/s41467-018-07557-4. https://doi.org/10.1038/s41467-018-07557-4.

Holmes, R. M., A. I. Shiklomanov, A. Suslova, M. Treriakov, J. W. McClelland, R. G. M. Spencer, and S. E. Tank. 2018. *Arctic Report Card 2018: River Discharge.* https://www.arctic.noaa.gov/Report-Card.

Holmes, R. M., A. I. Shiklomanov, A. Suslova, M. Tretiakov, J. W. McClelland, L. Scott, R. G. M. Spencer, and S. E. Tank. 2021. *Arctic Report Card 2021: River Discharge.* https://doi.org/10.25923/zevf-ar65.

Howard, Alan D., and Allen T. Hemberger. 1991. "Multivariate characterization of meandering." *Geomorphology* 4 (3-4): 161-186.

Hugelius, G., J. Strauss, S. Zubrzycki, J. W. Harden, E. A. G. Schuur, C. L. Ping, L. Schirrmeister, G. Grosse, G. J. Michaelson, C. D. Koven, J. A. O'Donnell, B. Elberling, U. Mishra, P. Camill, Z. Yu, J. Palmtag, and P. Kuhry. 2014. "Estimated stocks of circumpolar permafrost carbon with quantified uncertainty ranges and identified data gaps." *Biogeosciences* 11 (23): 6573-6593. https://doi.org/10.5194/bg-11-6573-2014. https://bg.copernicus.org/articles/11/6573/2014/.

Ielpi, Alessandro, Robert H. Rainbird, Dario Ventra, and Massimiliano Ghinassi. 2017. "Morphometric convergence between Proterozoic and post-vegetation rivers." *Nature*

Communications 8 (1): 15250. https://doi.org/10.1038/ncomms15250. https://doi.org/10.1038/ncomms15250.

IPCC. 2013. *Climate Change 2013: The Physical Science Basis. Contribution of Working Group I to the Fifth Assessment Report of the Intergovernmental Panel on Climate Change.* Cambridge University Press (Cambridge, United Kingdom and New York, NY, USA).

Jenkins, Liza K., Tom Barry, Karl R. Bosse, William S. Currie, Tom Christensen, Sara Longan, Robert A. Shuchman, Danielle Tanzer, and Jason J. Taylor. 2020. "Satellite-based decadal change assessments of pan-Arctic environments." *Ambio* 49 (3): 820-832. https://doi.org/10.1007/s13280-019-01249-z. https://doi.org/10.1007/s13280-019-01249-z.

Kanevskiy, Mikhail, Yuri Shur, Jens Strauss, Torre Jorgenson, Daniel Fortier, Eva Stephani, and Alexander Vasiliev. 2016. "Patterns and rates of riverbank erosion involving ice-rich permafrost (yedoma) in northern Alaska." *Geomorphology* 253: 370-384. https://doi.org/https://doi.org/10.1016/j.geomorph.2015.10.023. https://www.sciencedirect.com/science/article/pii/S0169555X15301872.

Kattsov, Vladimir M., John E. Walsh, William L. Chapman, Veronika A. Govorkova, Tatyana V. Pavlova, and Xiangdong Zhang. 2007. "Simulation and Projection of Arctic Freshwater Budget Components by the IPCC AR4 Global Climate Models." *Journal of Hydrometeorology* 8 (3): 571-589. https://doi.org/10.1175/jhm575.1. https://journals.ametsoc.org/view/journals/hydr/8/3/jhm575_1.xml.

Kaushal, Sujay S, Gene E Likens, Norbert A Jaworski, Michael L Pace, Ashley M Sides, David Seekell, Kenneth T Belt, David H Secor, and Rebecca L Wingate. 2010. "Rising stream and river temperatures in the United States." *Frontiers in Ecology and the Environment* 8 (9): 461-466. https://doi.org/https://doi.org/10.1890/090037. https://esajournals.onlinelibrary.wiley.com/doi/abs/10.1890/090037.

Kwok, R., and D. A. Rothrock. 2009. "Decline in Arctic sea ice thickness from submarine and ICESat records: 1958–2008." *Geophysical Research Letters* 36 (15). https://doi.org/https://doi.org/10.1029/2009GL039035. https://agupubs.onlinelibrary.wiley.com/doi/abs/10.1029/2009GL039035.

Landrum, Laura, and Marika M. Holland. 2020. "Extremes become routine in an emerging new Arctic." *Nature Climate Change* 10 (12): 1108-1115. https://doi.org/10.1038/s41558-020-0892-z. https://doi.org/10.1038/s41558-020-0892-z.

Lauer, J. Wesley, and Gary Parker. 2008a. "Modeling framework for sediment deposition, storage, and evacuation in the floodplain of a meandering river: Theory." *Water Resources Research* 44 (4). https://doi.org/https://doi.org/10.1029/2006WR005528. https://agupubs.onlinelibrary.wiley.com/doi/abs/10.1029/2006WR005528.

---. 2008b. "Net local removal of floodplain sediment by river meander migration." *Geomorphology* 96 (1): 123-149. https://doi.org/https://doi.org/10.1016/j.geomorph.2007.08.003. https://www.sciencedirect.com/science/article/pii/S0169555X07003881.

Leeder, M. R. 1973. "Fluviatile fining-upwards cycles and the magnitude of palaeochannels." *Geological Magazine* 110 (3): 265-276.

Lenssen, Nathan J. L., Gavin A. Schmidt, James E. Hansen, Matthew J. Menne, Avraham Persin, Reto Ruedy, and Daniel Zyss. 2019. "Improvements in the GISTEMP Uncertainty Model." *Journal of Geophysical Research: Atmospheres* 124 (12): 6307-6326. https://doi.org/https://doi.org/10.1029/2018JD029522. https://agupubs.onlinelibrary.wiley.com/doi/abs/10.1029/2018JD029522.

Leopold, Luna B., and M. Gordon Wolman. 1960. "River meanders." *Geological Society of America Bulletin* 71 (6): 769-793.

Lininger, K. B., and E. Wohl. 2019. "Floodplain dynamics in North American permafrost regions under a warming climate and implications for organic carbon stocks: A review and synthesis." *Earth-Science Reviews* 193: 24-44. https://doi.org/10.1016/j.earscirev.2019.02.024.

Lique, Camille, Marika M. Holland, Yonas B. Dibike, David M. Lawrence, and James A. Screen. 2016. "Modeling the Arctic freshwater system and its integration in the global system: Lessons learned and future challenges." *Journal of Geophysical Research: Biogeosciences* 121 (3): 540-566. https://doi.org/https://doi.org/10.1002/2015JG003120. https://agupubs.onlinelibrary.wiley.com/doi/abs/10.1002/2015JG003120.

Liu, Baozhong, Daqing Yang, Baisheng Ye, and Svetlana Berezovskaya. 2005. "Long-term open-water season stream temperature variations and changes over Lena River Basin in Siberia." *Global and Planetary Change* 48 (1): 96-111. https://doi.org/https://doi.org/10.1016/j.gloplacha.2004.12.007. https://www.sciencedirect.com/science/article/pii/S0921818105000603.

Love, Doris. 1970. "Subarctic and subalpine: where and what?" *Arctic and Alpine Research* 2 (1): 63-73.

Marcus, W. Andrew, and Mark A. Fonstad. 2010. "Remote sensing of rivers: the emergence of a subdiscipline in the river sciences." *Earth Surface Processes and Landforms* 35 (15): 1867-1872. https://doi.org/https://doi.org/10.1002/esp.2094. https://onlinelibrary.wiley.com/doi/abs/10.1002/esp.2094.

McClelland, J. W., R. M. Holmes, B. J. Peterson, and M. Stieglitz. 2004. "Increasing river discharge in the Eurasian Arctic: Consideration of dams, permafrost thaw, and fires as potential agents of change." *Journal of Geophysical Research: Atmospheres* 109 (D18). https://doi.org/https://doi.org/10.1029/2004JD004583. https://agupubs.onlinelibrary.wiley.com/doi/abs/10.1029/2004JD004583.

McClelland, James W., Stephen J. Déry, Bruce J. Peterson, Robert M. Holmes, and Eric F. Wood. 2006. "A pan-arctic evaluation of changes in river discharge during the latter half of the 20th century." *Geophysical Research Letters* 33 (6). https://doi.org/https://doi.org/10.1029/2006GL025753. https://agupubs.onlinelibrary.wiley.com/doi/abs/10.1029/2006GL025753.

McNamara, J. P., and D. L. Kane. 2009. "The impact of a shrinking cryosphere on the form of arctic alluvial channels." *Hydrological Processes* 23 (1): 159-168. https://doi.org/10.1002/hyp.7199. <Go to ISI>://WOS:000262397100011.

McNamara, James P. 2012. "Is There a Northern Signature on Fluvial Form?" In *Gravel-Bed Rivers*, 541-545.

McNamara, James P., Douglas L. Kane, and Larry D. Hinzman. 1997. "Hydrograph separations in an arctic watershed using mixing model and graphical techniques." *Water Resources Research* 33 (7): 1707-1719. https://doi.org/https://doi.org/10.1029/97WR01033. https://agupubs.onlinelibrary.wiley.com/doi/abs/10.1029/97WR01033.

---. 1998. "An analysis of streamflow hydrology in the Kuparuk River Basin, Arctic Alaska: a nested watershed approach." *Journal of Hydrology* 206 (1): 39-57. https://doi.org/https://doi.org/10.1016/S0022-1694(98)00083-3. https://www.sciencedirect.com/science/article/pii/S0022169498000833.

---. 1999. "An analysis of an arctic channel network using a digital elevation model." *Geomorphology* 29 (3): 339-353. https://doi.org/https://doi.org/10.1016/S0169-

555X(99)00017-3. https://www.sciencedirect.com/science/article/pii/S0169555X99000173.

Mudryk, L. R., P. J. Kushner, C. Derksen, and C. Thackeray. 2017. "Snow cover response to temperature in observational and climate model ensembles." *Geophysical Research Letters* 44 (2): 919-926. https://doi.org/https://doi.org/10.1002/2016GL071789. https://agupubs.onlinelibrary.wiley.com/doi/abs/10.1002/2016GL071789.

Nijssen, Bart, Greg M. O'Donnell, Alan F. Hamlet, and Dennis P. Lettenmaier. 2001. "Hydrologic Sensitivity of Global Rivers to Climate Change." *Climatic Change* 50 (1): 143-175. https://doi.org/10.1023/A:1010616428763. https://doi.org/10.1023/A:1010616428763.

Nowacki, Gregory J., Page Spencer, Michael Fleming, Terry Brock, and Torre Jorgenson. 2003. *Unified Ecoregions of Alaska: 2001*. (U.S. Geological Survey Open-File Report 02-297). http://pubs.er.usgs.gov/publication/ofr2002297.

Obu, Jaroslav, Sebastian Westermann, Annett Bartsch, Nikolai Berdnikov, Hanne H. Christiansen, Avirmed Dashtseren, Reynald Delaloye, Bo Elberling, Bernd Etzelmüller, Alexander Kholodov, Artem Khomutov, Andreas Kääb, Marina O. Leibman, Antoni G. Lewkowicz, Santosh K. Panda, Vladimir Romanovsky, Robert G. Way, Andreas Westergaard-Nielsen, Tonghua Wu, Jambaljav Yamkhin, and Defu Zou. 2019. "Northern Hemisphere permafrost map based on TTOP modelling for 2000–2016 at 1 km2 scale." *Earth-Science Reviews* 193: 299-316. https://doi.org/https://doi.org/10.1016/j.earscirev.2019.04.023. https://www.sciencedirect.com/science/article/pii/S0012825218305907.

Olson, David M., Eric Dinerstein, Eric D. Wikramanayake, Neil D. Burgess, George V. N. Powell, Emma C. Underwood, Jennifer A. D'amico, Illanga Itoua, Holly E. Strand, John C. Morrison, Colby J. Loucks, Thomas F. Allnutt, Taylor H. Ricketts, Yumiko Kura, John F. Lamoreux, Wesley W. Wettengel, Prashant Hedao, and Kenneth R. Kassem. 2001. "Terrestrial Ecoregions of the World: A New Map of Life on Earth: A new global map of terrestrial ecoregions provides an innovative tool for conserving biodiversity." *BioScience* 51 (11): 933-938. https://doi.org/10.1641/0006-3568(2001)051[0933:Teotwa]2.0.Co;2. https://doi.org/10.1641/0006-3568(2001)051[0933:TEOTWA]2.0.CO;2.

Overland, James, Edward Dunlea, Jason E. Box, Robert Corell, Martin Forsius, Vladimir Kattsov, Morten Skovgård Olsen, Janet Pawlak, Lars-Otto Reiersen, and Muyin Wang. 2019. "The urgency of Arctic change." *Polar Science* 21: 6-13.

https://doi.org/https://doi.org/10.1016/j.polar.2018.11.008. https://www.sciencedirect.com/science/article/pii/S1873965218301543.

Park, H., E. Watanabe, Y. Kim, I. Polyakov, K. Oshima, X. D. Zhang, J. S. Kimball, and D. Q. Yang. 2020. "Increasing riverine heat influx triggers Arctic sea ice decline and oceanic and atmospheric warming." *Science Advances* 6 (45): 7. https://doi.org/10.1126/sciadv.abc4699. <Go to ISI>://WOS:000587544300027.

Pavelsky, T. M., and L. C. Smith. 2008. "RivWidth: A Software Tool for the Calculation of River Widths From Remotely Sensed Imagery." *IEEE Geoscience and Remote Sensing Letters* 5 (1): 70-73. https://doi.org/10.1109/LGRS.2007.908305.

Payne, C., S. Panda, and A. Prakash. 2018. "Remote Sensing of River Erosion on the Colville River, North Slope Alaska." *Remote Sensing* 10 (3): 20. https://doi.org/10.3390/rs10030397. <Go to ISI>://WOS:000428280100043.

Peterson, Bruce J., Robert M. Holmes, James W. McClelland, Charles J. Vörösmarty, Richard B. Lammers, Alexander I. Shiklomanov, Igor A. Shiklomanov, and Stefan Rahmstorf. 2002. "Increasing River Discharge to the Arctic Ocean." *Science* 298 (5601): 2171-2173. https://doi.org/10.1126/science.1077445. https://science.sciencemag.org/content/sci/298/5601/2171.full.pdf.

Prowse, T. 1994. "Environmental significance of ice to streamflow in cold regions." *Freshwater Biology* 32 (2): 241-259. https://doi.org/https://doi.org/10.1111/j.1365-2427.1994.tb01124.x. https://onlinelibrary.wiley.com/doi/abs/10.1111/j.1365-2427.1994.tb01124.x.

Prowse, T., A. Bring, J. Mård, E. Carmack, M. Holland, A. Instanes, T. Vihma, and F. J. Wrona. 2015. "Arctic Freshwater Synthesis: Summary of key emerging issues." *Journal of Geophysical Research: Biogeosciences* 120 (10): 1887-1893. https://doi.org/https://doi.org/10.1002/2015JG003128. https://agupubs.onlinelibrary.wiley.com/doi/abs/10.1002/2015JG003128.

Rawlins, Michael A., Michael Steele, Marika M. Holland, Jennifer C. Adam, Jessica E. Cherry, Jennifer A. Francis, Pavel Ya Groisman, Larry D. Hinzman, Thomas G. Huntington, and Douglas L. Kane. 2010. "Analysis of the Arctic system for freshwater cycle intensification: Observations and expectations." *Journal of Climate* 23 (21): 5715-5737.

Raynolds, Martha K., Donald A. Walker, Andrew Balser, Christian Bay, Mitch Campbell, Mikhail M. Cherosov, Fred J. A. Daniëls, Pernille Bronken Eidesen, Ksenia A. Ermokhina, Gerald V. Frost, Birgit Jedrzejek, M. Torre Jorgenson, Blair E. Kennedy, Sergei S. Kholod, Igor A. Lavrinenko, Olga V. Lavrinenko, Borgþór Magnússon, Nadezhda V. Matveyeva, Sigmar Metúsalemsson, Lennart Nilsen, Ian Olthof, Igor N. Pospelov, Elena B. Pospelova, Darren Pouliot, Vladimir Razzhivin, Gabriela Schaepman-Strub, Jozef Šibík, Mikhail Yu Telyatnikov, and Elena Troeva. 2019. "A raster version of the Circumpolar Arctic Vegetation Map (CAVM)." *Remote Sensing of Environment* 232: 111297. https://doi.org/https://doi.org/10.1016/j.rse.2019.111297. https://www.sciencedirect.com/science/article/pii/S0034425719303165.

Rew, L. J., K. L. McDougall, J. M. Alexander, C. C. Daehler, F. Essl, S. Haider, C. Kueffer, J. Lenoir, A. Milbau, M. A. Nunez, A. Pauchard, and W. Rabitsch. 2020. "Moving up and over: redistribution of plants in alpine, Arctic, and Antarctic ecosystems under global change." *Arctic Antarctic and Alpine Research* 52 (1): 651-665. https://doi.org/10.1080/15230430.2020.1845919. <Go to ISI>://WOS:000601401000001.

Rigor, Ignatius G, Roger L Colony, and Seelye Martin. 2000. "Variations in surface air temperature observations in the Arctic, 1979–97." *Journal of Climate* 13 (5): 896-914. https://doi.org/https://doi.org/10.1175/1520-0442(2000)013<0896:VISATO>2.0.CO;2.

Rowland, Joel C., Eitan Shelef, Paul A. Pope, Jordan Muss, Chandana Gangodagamage, Steven P. Brumby, and Cathy J. Wilson. 2016. "A morphology independent methodology for quantifying planview river change and characteristics from remotely sensed imagery." *Remote Sensing of Environment* 184: 212-228.

Rowland, Joel C., and Sophie Stauffer. 2019. Pan-arctic river bank erosion and accretion, and planform metrics measured over intervals ranging from 1973 to 2016. In *Incorporating the Hydrological Controls on Carbon Cycling in Floodplain Ecosystems into Earth System Models (ESMs)*. United States: ESS-DIVE repository https://data.ess-dive.lbl.gov/datasets/doi:10.15485/1571527

Sayre, Roger, Jack Dangermond, Charlie Frye, Randy Vaughan, Peter Aniello, Sean P. Breyer, Douglas Cribbs, Dabney Hopkins, Richard Nauman, William Derrenbacher, Dawn J. Wright, Clint Brown, Charles Convis, Jonathan H. Smith, Laurence Benson, D. Paco VanSistine, Harumi Warner, Jill Janene Cress, Jeffrey J. Danielson, Sharon L. Hamann, Thomas Cecere, Ashwan D. Reddy, Devon Burton, Andrea Grosse, Diane True, Marc Metzger, Jens Hartmann, Nils Moosdorf, Hans Durr, Marc Paganini, Pierre Defourny, Olivier Arino, Simone Maynard, Mark Anderson, and Patrick Comer. 2014. *A new map of global ecological land units—An ecophysiographic stratification approach*. Association of American Geographers.

Schumm, S. A. 1967. "Meander wavelength of alluvial rivers." *Science* 157 (3796): 1549-1550.

Schwenk, Jon, Ankush Khandelwal, Mulu Fratkin, Vipin Kumar, and Efi Foufoula-Georgiou. 2017. "High spatiotemporal resolution of river planform dynamics from Landsat: The RivMAP toolbox and results from the Ucayali River." *Earth and Space Science* 4 (2): 46-75.

Scott, Kevin M. 1978. Effects of permafrost on stream channel behavior in arctic Alaska, U.S. Geological Survey Professional Paper 1068. U.S. Government Printing Office.

Serreze, Mark C., and Roger G. Barry. 2011. "Processes and impacts of Arctic amplification: A research synthesis." *Global and Planetary Change* 77 (1): 85-96. https://doi.org/https://doi.org/10.1016/j.gloplacha.2011.03.004. https://www.sciencedirect.com/science/article/pii/S0921818111000397.

Stølum, Hans-Henrik. 1998. "Planform geometry and dynamics of meandering rivers." *Geological Society of America Bulletin* 110 (11): 1485-1498.

Stroeve, J. C., M. C. Serreze, M. M. Holland, J. E. Kay, J. Malanik, and A. P. Barrett. 2012. "The Arctic's rapidly shrinking sea ice cover: a research synthesis." *Climatic Change* 110 (3-4): 1005-1027. https://doi.org/10.1007/s10584-011-0101-1. <Go to ISI>://WOS:000299346900026.

Thellman, Audrey, Kathi Jo Jankowski, Brian Hayden, Xiao Yang, Wayana Dolan, Adrianne P. Smits, and Antóin M. O'Sullivan. 2021. "The Ecology of River Ice." *Journal of Geophysical Research: Biogeosciences* 126 (9): e2021JG006275. https://doi.org/https://doi.org/10.1029/2021JG006275. https://agupubs.onlinelibrary.wiley.com/doi/abs/10.1029/2021JG006275.

van Vliet, M. T. H., F. Ludwig, J. J. G. Zwolsman, G. P. Weedon, and P. Kabat. 2011. "Global river temperatures and sensitivity to atmospheric warming and changes in river flow." *Water Resources Research* 47 (2). https://doi.org/https://doi.org/10.1029/2010WR009198. https://agupubs.onlinelibrary.wiley.com/doi/abs/10.1029/2010WR009198.

Vandenberghe, Jef, and Ming-ko Woo. 2002. "Modern and ancient periglacial river types." *Progress in Physical Geography: Earth and Environment* 26 (4): 479-506. https://doi.org/10.1191/0309133302pp349ra. https://doi.org/10.1191/0309133302pp349ra.

Whitefield, Jonathan, Peter Winsor, James McClelland, and Dimitris Menemenlis. 2015. "A new river discharge and river temperature climatology data set for the pan-Arctic region." *Ocean Modelling* 88: 1-15. https://doi.org/https://doi.org/10.1016/j.ocemod.2014.12.012. https://www.sciencedirect.com/science/article/pii/S1463500315000025.

Whiteman, Gail, Chris Hope, and Peter Wadhams. 2013. "Vast costs of Arctic change." *Nature* 499 (7459): 401-403. https://doi.org/10.1038/499401a. https://doi.org/10.1038/499401a.

Wild, Birgit, August Andersson, Lisa Bröder, Jorien Vonk, Gustaf Hugelius, James W. McClelland, Wenjun Song, Peter A. Raymond, and Örjan Gustafsson. 2019. "Rivers across the Siberian Arctic unearth the patterns of carbon release from thawing permafrost." *Proceedings of the National Academy of Sciences* 116 (21): 10280-10285.

Yang, Xiao, Tamlin M. Pavelsky, and George H. Allen. 2020. "The past and future of global river ice." *Nature* 577 (7788): 69-73. https://doi.org/10.1038/s41586-019-1848-1. https://doi.org/10.1038/s41586-019-1848-1.

Zeng, Heqing, Gensuo Jia, and Howard Epstein. 2011. "Recent changes in phenology over the northern high latitudes detected from multi-satellite data." *Environmental Research Letters* 6 (4): 045508. https://doi.org/https://doi.org/10.1088/1748-9326/6/4/045508.

Zhang, T., R. G. Barry, K. Knowles, J. A. Heginbottom, and J. Brown. 1999. "Statistics and characteristics of permafrost and ground-ice distribution in the Northern Hemisphere." *Polar Geography* 23 (2): 132-154. https://doi.org/10.1080/10889379909377670. https://doi.org/10.1080/10889379909377670.

Zhang, Xiangdong, Juanxiong He, Jing Zhang, Igor Polyakov, Rüdiger Gerdes, Jun Inoue, and Peili Wu. 2013. "Enhanced poleward moisture transport and amplified northern high-latitude wetting trend." *Nature Climate Change* 3 (1): 47-51. https://doi.org/10.1038/nclimate1631. https://doi.org/10.1038/nclimate1631.

Zheng, Lei, Irina Overeem, Kang Wang, and Gary D. Clow. 2019. "Changing Arctic River Dynamics Cause Localized Permafrost Thaw." *Journal of Geophysical Research: Earth Surface* 124 (9): 2324-2344. https://doi.org/10.1029/2019jf005060.

Zinger, Jessica A., Bruce L. Rhoads, and James L. Best. 2011. "Extreme sediment pulses generated by bend cutoffs along a large meandering river." *Nature Geoscience* 4 (10): 675-678. https://doi.org/10.1038/ngeo1260. https://doi.org/10.1038/ngeo1260.